NTNU

Norwegian University of
Science and Technology

Analysis and Design Bjørnefjorden Floating Cable-Stayed Bridge subjected to Large Ship Collisions and Extreme Environmental Loads

Boya Wang

Maritime Engineering
Submission date: June 2017
Supervisor: Jørgen Amdahl, IMT
Co-supervisor: Jonas Ringsberg, Chalmers University of Technology
Yanyan Sha, IMT

Norwegian University of Science and Technology
Department of Marine Technology

NTNU – Trondheim
Norwegian University of
Science and Technology

Analysis and Design Bjørnefjorden Floating Cable-Stayed Bridge subjected to Large Ship Collisions and Extreme Environmental Loads

Boya Wang

June 2017

MASTER THESIS

Department of Marine Technology

Norwegian University of Science and Technology

Supervisor: Professor Jørgen Amdahl

NTNU
Norges teknisk-naturvitenskapelige universitet
Institutt for marin teknikk

MASTER THESIS 2017

For

Stud. Techn. Boya Wang.

Analysis and Design Bjørnefjorden Floating Cable-Stayed Bridge subjected to Large Ship Collisions and Extreme Environmental Loads

Analyse og dimensjonering Bjørnefjorden flytende skråstagbro utsatt for støt fra store skip og ekstreme miljølaster

The Norwegian Public Roads Administration (NPRA) is running a project "Ferry free coastal route E39", where suspension bridges, floating bridges or submerged tunnels would be installed across fjords in Western Norway. The straits are up 5 kilometres wide and will call for significant extension of present technology. Several innovative crossing concepts have been proposed. One of them is the combined floating-cable stayed bridge concept.

The bridge has to resist extreme environmental loads and accidental actions with acceptable safety levels. One of the concerns are accidental ship collisions with energies 100-1500 MJ. The proposed concepts cannot be designed adequately using existing methods and design rules. Consequently, advanced scenario-based analyses have to be conducted based on accurate simulation of the governing physical processes.

For crossing of Bjørnefjorden one of the most relevant concept is floating bridge with a cable stayed section.

The purpose of the project and (later) master thesis work is to perform scenario-based and advanced analysis of ship collision with the bridge and to assess the response of the bridge exposed to extreme environmental loads, both in intact and damaged condition.

.

Scope of work:

1. Perform parametric study of ship collision analysis for selected scenarios against the pontoons and the bridge girder. Pontoons fabricated in both concrete and steel should be considered. For bridge girder impact the effect of local damage on the global girder resistance should be modelled ain USFOS as far as possible. Assess the criticality of the bridge response wrt to global integrity.

2. By means of analysis with LS-DYNA propose a pontoon steel design that is highly resistant against ship collision.

3. Simulate non-central impacts with the pontoons where the ship may be deflected away from the pontoon

4. Establish relevant environmental conditions for the bridge. To what extent can USFOScalculate the environmental loads? If need be, use alternative software (e.g. WADAM) to calculate the environmental loads, notably wave loads including drift forces. Reference is made to the master thesis by Ole Harald Moe. Turbulent wind may be created with the program WINDSIM.

5. Analyse the bridge subjected to extreme environmental loads, using e.g. the contour line method. Establish the extreme characteristic response and compare with relevant resistance criteria.

6. For selected damage condition as concerns girder damage or pontoon flooding, assess the residual strength of the bridge subjected to relevant environmental loads

7. Conclusions and recommendations for further work in the master thesis project

Literature studies of specific topics relevant to the thesis work may be included.

The work scope may prove to be larger than initially anticipated. Subject to approval from the supervisor, topics may be deleted from the list above or reduced in extent.

In the thesis the candidate shall present his personal contribution to the resolution of problems within the scope of the thesis work.

Theories and conclusions should be based on mathematical derivations and/or logic reasoning identifying the various steps in the deduction.

The candidate should utilise the existing possibilities for obtaining relevant literature.

The thesis should be organised in a rational manner to give a clear exposition of results, assessments, and conclusions. The text should be brief and to the point, with a clear language. Telegraphic language should be avoided.

The thesis shall contain the following elements: A text defining the scope, preface, list of contents, summary, main body of thesis, conclusions with recommendations for further work, list of symbols and acronyms, references and (optional) appendices. All figures, tables and equations shall be numerated.

The supervisor may require that the candidate, in an early stage of the work, presents a written plan for the completion of the work. The plan should include a budget for the use of computer and laboratory resources, which will be charged to the department. Overruns shall be reported to the supervisor.

The original contribution of the candidate and material taken from other sources shall be clearly defined. Work from other sources shall be properly referenced using an acknowledged referencing system.

The report shall be submitted in two copies:

- Signed by the candidate
- The text defining the scope included
- In bound volume(s)
- Drawings and/or computer prints, which cannot be bound, should be organised in a separate folder.

Supervisor:
Prof. Jørgen Amdahl

Co-supervisor:
Postdoc Yanyan Sha

Deadline:, June 10, 2017

Trondheim, January 11, 2017

Jørgen Amdahl

Preface

This Master's Thesis is the result of the work done by student Boya Wang at the Norwegian University of Science and Technology during the spring of 2017. The scope of work was developed by Professor Jørgen Amdahl and builds on the Project Thesis written during the fall of 2016.

I would like to give a special thanks to Professor Jørgen Amdahl for supervising the work done and providing many rewarding discussions during the process. The help from Post. Doc Yanyan Sha was also very important, especially with Patran modelling and the USFOS analyses. I would also thank Jonas Ringsberg, my supervisor at Chalmers University of Technology, for helping through the thesis work when I was in Norway. Last but not the least important, I appreciate the supports that my friends and my parents give me, either in work or in life, without you I can not have a great life studying in Norway.

This project is supported by Norwegian Public Roads Administration, The main purpose of the project is to analyze ship collision with a floating bridge for crossing of Bjørnefjorden. Since the information of the project is private property, some of the detailed drawings and models are not included, if one wants to further use the materials of the model, please contact the author of this thesis.

Trondheim, 2017-06-01

Boya Wang

Contents

List of Figures

List of Tables

Nomenclature

ϵ_{cr}	Critical strain
ϵ_{cr}	Failure strain
ϵ_{UTS}	Ultimate strain
λ	Thermal expansion coefficient
μ	Poisson's ratio
σ	Stress
a	Added mass
B	Bulk modulus
C	Damping force
E	Elastic modulus
E_s	Strain energy
F	Force
G	Shear modulus
I	Moment of inertia
K	Stiffness
k	Power law parameter
l_e	Mesh length

M	Moment
m	Mass
n	Power law parameter
S	Cross section area of bridge girder
T	Temperature
t_e	Mesh thickness
T_n	Natural period
v	Velocity
x	Displacement
y	Distance to the plastic neutral axis
Z	Plastic modulus

Abstract

The highway E39 project is proposed by Norwegian Highway Authority (NPRA), it will connect Trondheim to Kristiansand with bridges building on the fjords. Due to the large span length and the depth of the water of the fjords, the floating bridge concept is proposed. The bridge will be supported by the pontoons floating on the water. In the navigation channel, there are two towers with the cables connecting the bridge girder. In reality, this bridge has a larger possibility of experiencing ship collisions. In this thesis, the local ship bow and pontoon is conducted to propose a safe pontoon design, then the global analysis of the bridge under ship collision has been done.

A pontoon steel design that is highly resistant against ship collision is investigated. After obtaining the safe design of the pontoon, collision simulations are conducted between a container ship and the pontoon in order to obtain the force deformation curve for the ship. The force deformation curve is an essential input when doing the global analysis of the bridge since the contact force between the ship and pontoon is predicted based on the curve.

The global response of the bridge that subjected to ship collision is analyzed in USFOS, where the finite element model of an entire bridge is built. The ship is modelled as mass spring system with given velocity. The original bridge model has been improved by adding the pre-tension in the cables and checking the balance of the bridge.

Four different cases are investigated where the ship has different sailing direction and sailing speed. The difference in the first two cases is that they have different ship speed with collision energy 158.4MJ and 440MJ respectively. The third and forth cases have different collision angel relative to the pontoon, however they have the same collision energy 440MJ.

The transverse displacement of the bridge ranges from 2.4m to 3.4m in the four cases. The results of the transverse displacement obtained in USFOS are quite close to the value from hand calculation of single degree of freedom. The collision force in the four cases is quite similar, the average value of the contact force is around 35MN. The absorbed energy by the ship ranges from 66% to 72%, the ship would drift away from the bridge. The largest spring permanent deformation is 9m, it happens in the forth case, where there is a small angel between the ship

and pontoon.

The response of the bridge deck that right upon the ship is investigated. It is found out the transverse bending moment is relatively large, because the ship-bridge collision happens at the middle point of the bridge, it is easy to trigger large transverse bending moment.

The bridge design needs to be modelled with more details, some assumptions have been made, so the analysis of the bridge is conservative.

Chapter 1

Introduction

From autopilot to high-speed rail, road traffic has become more and more convenient over the past few years. Norway, a country with advanced technology and innovation, plans to spend 25 billion US dollars in building a coastal route which links Kristiansand and Trondheim so that cars can travel on.

1.1 Background

In 2014, in order to reduce travel time, the Norwegian Highway Authority (NPRA) proposed a highway project "Highway E39" built on the west coast of Norway. E39 will connect from Kristiansand to Trondheim, which will greatly enhance the speed of transport in the western cities of Norway and will have a greater boost to economic growth. The Norwegian government plans to complete building the highway E39 within 20 years, as shown in Figure 1.2.

There are some difficulties if one wants to build a traditional bridge across the fjord due to the huge span length and the depth of water, in addition, the extreme weather conditions in the area also needs to be considered. In this case, several concepts of bridge have been proposed, such as span suspension bridge, submerged tunnel, pontoon floating bridge, or a combination of the above three.

For the span suspension bridges, the advantage is it can use relatively little material to span a

Figure 1.1: E39 Fjorden crossings. Reprinted from Vegvesen (2015)

relatively long distance. Suspension bridge can be made relatively high, allowing the ships going through. However, there are several disadvantages of the span suspension bridge. The tower of the suspension bridge exerts a very large force on the ground, so if the ground itself is relatively soft, the foundation of the tower must be very large and quite expensive.

For submerged tunnel, it allows the ship going through compared with the low bridges and it will not be affected by the harsh wind. However, tunnels require far higher costs of security and construction than bridges.

Another concept is the floating bridges with pontoons, this kind of bridge can avoid the need of one large span. However, it increases the possibility of ship collisions, especially in extreme environmental conditions.

The proposed bridge in this project is a 4198 meter long curved floating bridge with a cable stayed section in the middle of the bridge. The middle part of the bridge is designed with two towers with cables connecting the girders, this part is mainly for the ship traffic. There are two girders connected by the beams to provide a better service for the traffic. The bridge is supported

by 20 concrete pontoons with ballast water in. The two ends of the bridge are fixed, the other parts of the bridge are not. The bridge is shown in figure 1.2.

Figure 1.2: E39 Fjorden crossings. Reprinted from Vegvesen (2015)

1.2 Motivation

As the global trade continues to grow in recent years, more and more ships are sailing. It is increasingly challenging to avoid ship accidents, such as collisions. The International Maritime Organization (IMO) reported an average of 23.8 ship collisions happens over the past 10 years with very serious consequences (Storheim (2016)). The consequences of the ship collisions can be very serious, including loss of life and serious environmental pollution, it is quite important to predict the outcome of the ship collisions.

The most famous ship collision may be the Titanic collision with the iceberg. In 1912, the Titanic collided with an iceberg when it was sailing to New York. The result of this event was severe due to the loss of human life and the properties and this event has affected the improvement of the ship regulation significantly. Since then, the accidental events are considered when designing the ships, such as ship collision, flooding etc.

In addition to the collision of ships and ships, in recent years due to the increasingly heavy traffic at sea, ship and bridge collision accidents often occur. From the world's statistical data analysis, in the navigation of large bridges during operation, probably 10% of the bridge will be damaged due to the impact of the ship. According to Wang (2000), during the period from 1919 to 1990, there were 73 ship collapses in Nanjing, Jiujiang, Wuhan and Zhicheng on the Yangtze River in China, resulting in serious losses of people and property.

1.3 Objectives

As the work goes on, the scope of the total work has therefore been modified to focus on the ship collision because the modelling of the pontoon in Patran takes far more time than estimated. The tasks concerning the environmental loads can be regarded as future work under discussion with supervisor Jørgen Amdahl. The thesis work focus on the following objectives:

- Propose a pontoon steel design that is highly resistant against ship collision by using Patran and LS-DYNA. Carry out analysis of the ship-pontoon collision in LS-DYNA to obtain the ship's force-deformation curve.
- Analyze the global response of the Bjørnefjorden bridge that subjected to the ship collision where the force-deformation curve obtained from LS-DYNA is used to provide the ship collision properties. Different collision angels are investigated.

1.4 Previous Work

During the fall semester in 2016, a project thesis has been conducted in order to provide a foundation for this master thesis. A finite element model of the Bjørnefjorden bridge was established and the modal study of the bridge was conducted in USFOS. A simplified hand calculation for response estimation of Single Degree of Freedom system was made to compare with the results obtained from the finite element method simulation. The project thesis is reported in Wang (2016), some detailed modelling of the bridge can be referred to this report.

Chapter 2

Theory

2.1 Theory of Collision

2.1.1 Previous Work of Ship Collision

In general, the methods for ship collision analysis are finite element method, simplified analytical method and experimental or empirical method, according to Hong and Amdahl (2008).

The finite element method, i.e the numerical simulation method is a widely used method today. Haris and Amdahl (2013) firstly analyze the collision damage of two ships by numerical simulations method, then it is verified that the experimental data match the results from the numerical simulations method . In this case, the finite element simulation is a reliable method when there is a lack of the experimental data. Hagiwara et al. (1983) has proposed a highly accurate method for predicting the ship collision damage, especially for the low energy collisions. In Petersen (1982), the procedures for simulating dynamic analysis of the ship collision are presented, the non-linear system equations are solved by numerical time integration method.

The experimental or empirical method is also an important method for ship collision. To ensure there are enough experimental data to rely on, Vredeveldt and Wevers (1993) has conducted a series of collision experiments with two tankers with around 1000 tonnes displacement. Many valuable results are obtained such as the collision force, ship motions after collision and the

strains in the ship due to collision. Ohtsubo et al. (1994) has investigated ship collision and grounding of oil tankers by full scale experiments, after comparison with the numerical work, some newly developed code has been added into the numerical simulation. Tabri et al. (2009) obtained the internal mechanics from full scale experiments in two conditions, one considered the effect of the sloshing effect and the other one did not consider. The predictions from theoretical model is in good agreement with the results from the experiments.

2.1.2 Ship Collision Theory

Several regulations about the ship collision are established and widely used such as DNV-RP-C204 and Eurocode. The one often used in Nodic countries is NORSOK N004.

There are two mechanisms to analyze the collision process. One is the external mechanics, it mainly focuses on how much energy has dissipated as strain energy. Another is internal mechanics, it deals with how the dissipated energy distributed in the striking and struck part.

For the external mechanic, the main principle to calculate how much energy that dissipates as strain energy is the conservation of momentum and the conservation of the energy, (DNV-RP-C204 (2010)). The conservation of momentum and energy is shown in equation 2.1 and equation 2.2.

$$(m_s + a_s)v_s + (m_b + a_b)v_b = (m_s + a_s + m_b + a_b)V \tag{2.1}$$

$$\frac{1}{2}(m_s + a_s)v_s^2 + \frac{1}{2}(m_b + a_b)v_b^2 = \frac{1}{2}(m_s + a_s + m_b + a_b)V^2 + E_s \tag{2.2}$$

where

m_s is ship mass

a_s is added mass of the ship

v_s is ship speed m_b is mass of the bridge

a_b is added mass of the bridge

v_b is bridge speed

V is velocity of ship and bridge after collision

E_s is the strain energy.

Here it is assumed the ship and bridge have the same speed after collision, that is V. Then the strain energy E_s can be calculated. The strain energy dissipated by the ship and the bridge equals to the total area under the load deformation curves, figure 2.1.

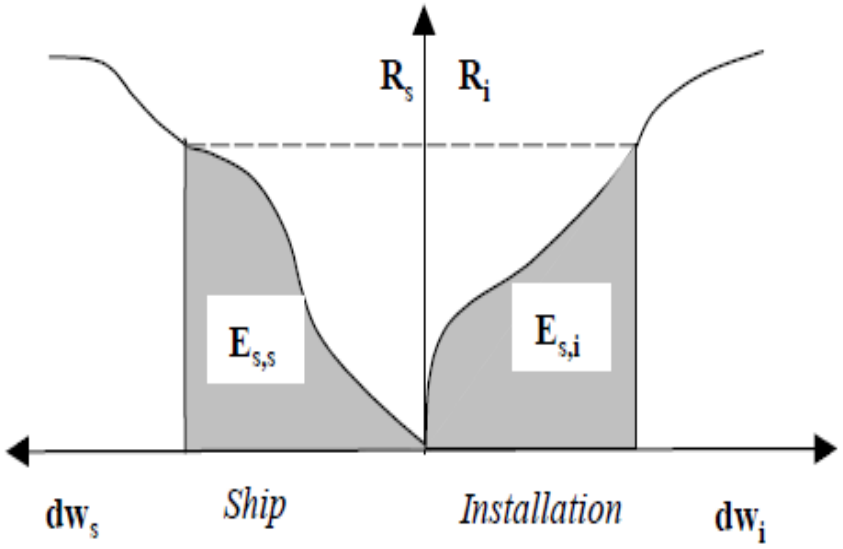

Figure 2.1: Dissipation of strain energy in ship and bridge. Reprinted from DNV-RP-C204 (2010)

The strain energy can be calculated by equation 2.3.

$$E_s = E_{s,s} + E_{s,b} = \int_0^{W_{s,max}} R_s dw_s + \int_0^{W_{d,max}} R_d dw_d \tag{2.3}$$

How the dissipated energy is distributed is solved in Internal Mechanism. According to DNV-RP-C204 (2010), there are three design stages: strength design, ductility design and the shared-energy design, shown in figure 2.2. From the figure, in the strength design, the energy dissipation for the ship is much higher than that in bridge, meaning most of the strain energy is dissipated in the ship and little in the bridge or pontoon. In this case, the pontoon can be regarded as rigid body, but it may result in over strengthened pontoon. In the ductile design, it is the opposite

condition of the strength design, the ship can be regarded as rigid body and have small deformation since the bridge will contribute most of the dissipated energy and has relatively large plastic deformation. In shared-energy design, both the ship and the bridge contribute to the energy dissipate and have large deformations, this is the most reasonable condition.

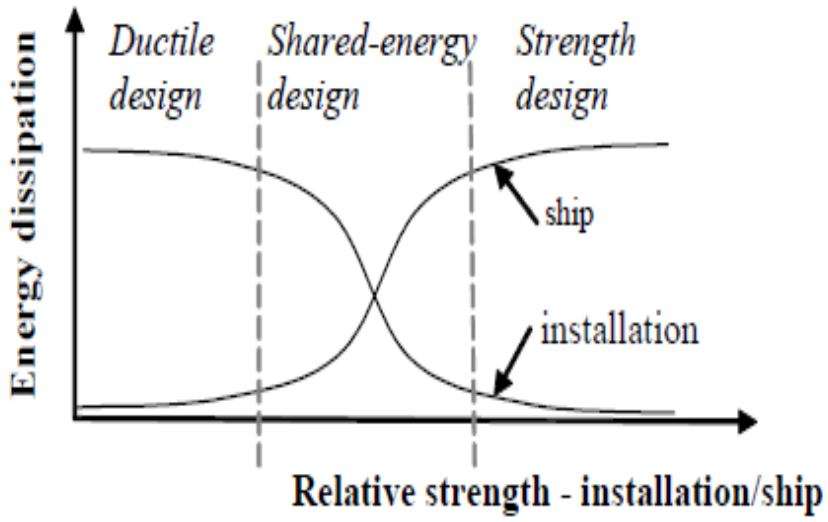

Figure 2.2: Energy dissipation for three designs. Reprinted from DNV-RP-C204 (2010)

2.2 Review of the Finite Element Method

Finite element method is widely used in engineering design of ships, offshore structures, buildings etc. Usually the engineering problem is too complicated to be solved by classic analytic method so that the numerical method FEM is used. The main procedures of FEM is shown as follows according to Moan (2003).

1. Discretisation. The main structure area is divided into small elements by meshing. The connected elements share the same nodes. The mesh size and number of elements are very important to the result.

2. Find the equilibrium relationship between the forces, moments and the displacements within one element.

3. For the whole system, the equilibrium between the displacement and the load for all the nodes needs to be established.

4. The boundary conditions are used after the equilibrium of the whole system is established.

5. The global matrices of the global displacement are obtained by solving the equilibrium equation.

6. After the equation has been solved for the whole system, any nodal displacement can be expressed by the interpolation functions. Then the stresses can be expressed by the nodal displacements directly combined with Hooke's Law.

In some cases, due to the boundary conditions and the nonlinear of the material, the linear method is no longer valid.

2.3 Soving Dynamic Equations of Motion

The dynamic response of a structure with respect to an external load can be expressed by the dynamic equilibrium equation, written as Eq. 2.4.

$$M\ddot{x} + C\dot{x} + Kx = R \tag{2.4}$$

Where M, C and K demotes the matrix of inertia forces, damping forces and structural stiffness; $\ddot{x}$,$\dot{x}$ and x denotes the nodal acceleration, velocity and displacement respectively. R represents the external loads.

Depending on the features of the applied load and the structure response, two types of analysis can be performed to solve the above equation, i.e. frequency domain analysis and time domain analysis. If both the load and response are in linear relationship, the frequency domain analysis can be prescribed. Otherwise, the time domain analysis must be applied for non-linear conditions. In this thesis, the impulse ship collision is considered to be a non-linear external load, therefore the dynamic equilibrium equation is solved in the time domain.

In time domain analysis, the structural response is solved in an iterative procedure. Provided with the load and properties ($\ddot{x}\ \dot{x}\ x$) in the initial time step, the response for the next time step can be computed based on the information in the previous time step. Gradually, the whole response history in the time domain is obtained by time step increments. In the USFOS software, the time integration adopts a Hilbert-Hughes-Taylor-α (HHT-α) method which is an enhanced form of the Newmark-β method. The HHT-α method introduces a damping parameter α to maintain the solver stability and accuracy. This is mainly beneficial to the higher frequency modes which are frequently unstable according to Tore H. Soreide and Hellam (1993).

Chapter 3

Local Ship Bow-Pontoon Collision Analysis

When analyzing the global response of a structure, the structure as a whole would need to be included in the model. However, due to the large number of elements and the expensive cost of calculation time, it is acceptable that the whole structure can be simplified if the local analysis appears to be more important.

In this thesis, two models are built. One is the local model representing the collision between the ship bow and the pontoon, one is the global model of the bridge to simulate the global response after obtaining force-displacement curve from the local model simulation.

The modelling of ship-pontoon collision is done in Patran and Ls Dyna and the whole bridge modelling is done using USFOS.

3.1 Geometry Modelling

The geometry of the pontoon is shown in Figure 3.1. Since ship-pontoon collision only occurs at the "half circle" part of the pontoon, considering the calculation time, it is easier to only model the collision part of the pontoon.

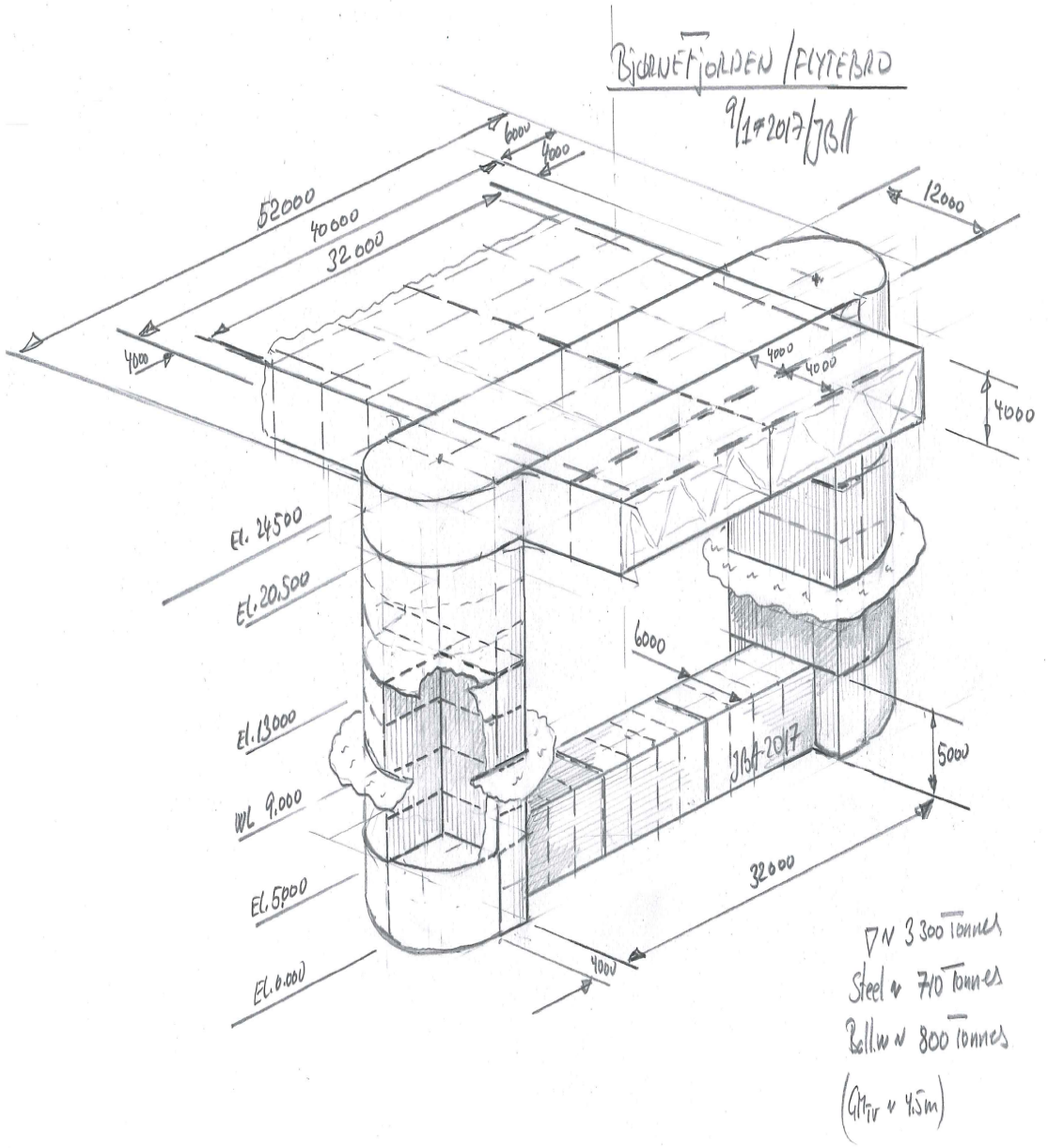

Figure 3.1: Pontoon

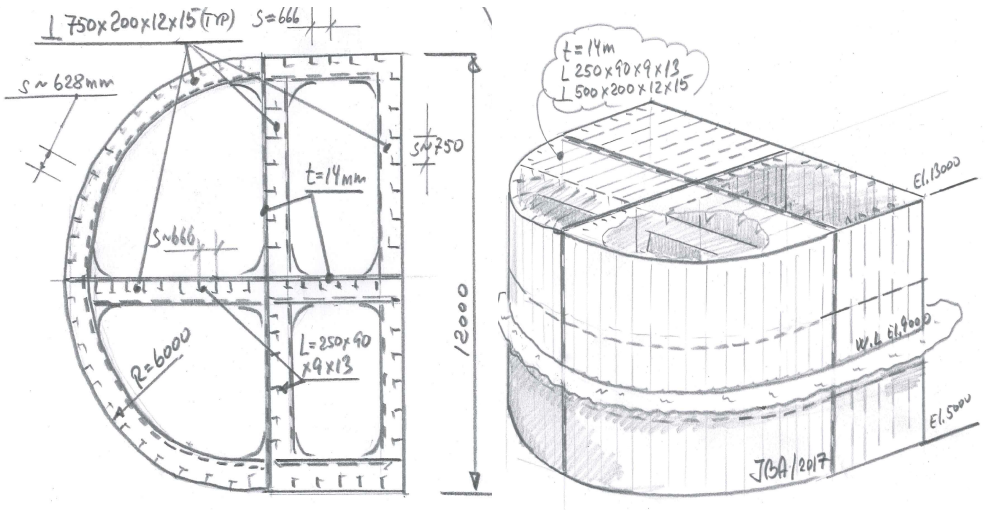

(a) Top view of the pontoon (b) Pontoon height of 5-13m

Figure 3.2: Different views of the pontoon

As mentioned earlier, the geometry modeling was performed in Patran. From the given figures, the modelling can be divided into several steps:

1. Modelling the girders including the longitudinal girders and the horizontal girders that support the decks, shown in figure 3.3.
2. Modelling the frames and inside plates, shown in figure 3.4.
3. Modelling the outer surfaces of the pontoon, shown in figure 3.5.
4. Modelling the horizontal decks, shown in figure 3.6.

In order to have a continuous mesh, an important procedure is to break every junction part of the model.

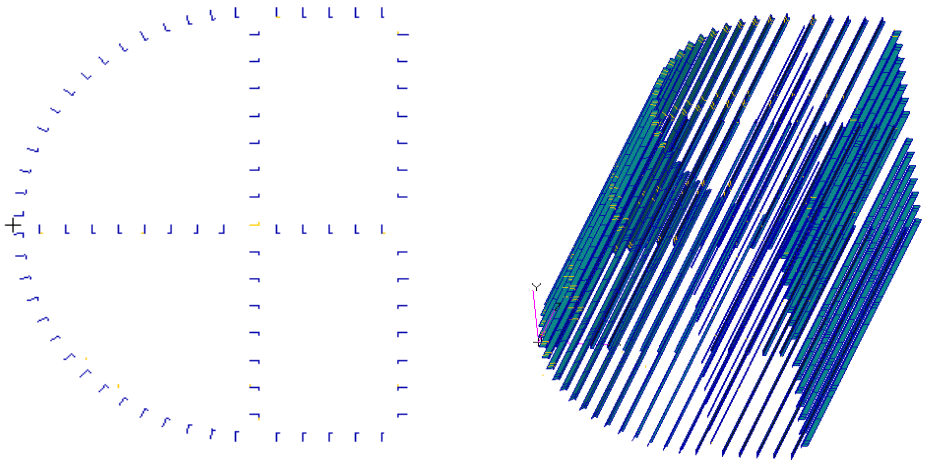

(a) Top view of step 1 (b) Arbitrary view of step 1

Figure 3.3: Step 1: Girder modelling

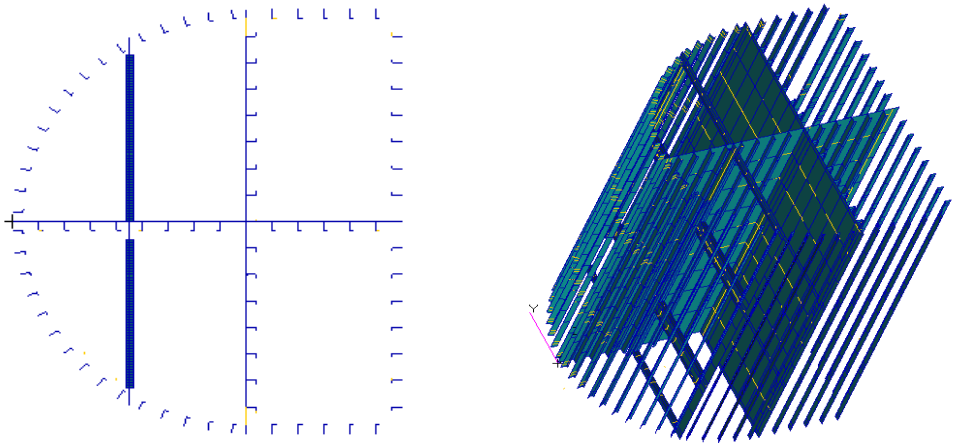

(a) Top view of step 2 (b) Arbitrary view of step 2

Figure 3.4: Step 2: Inner plate and frame

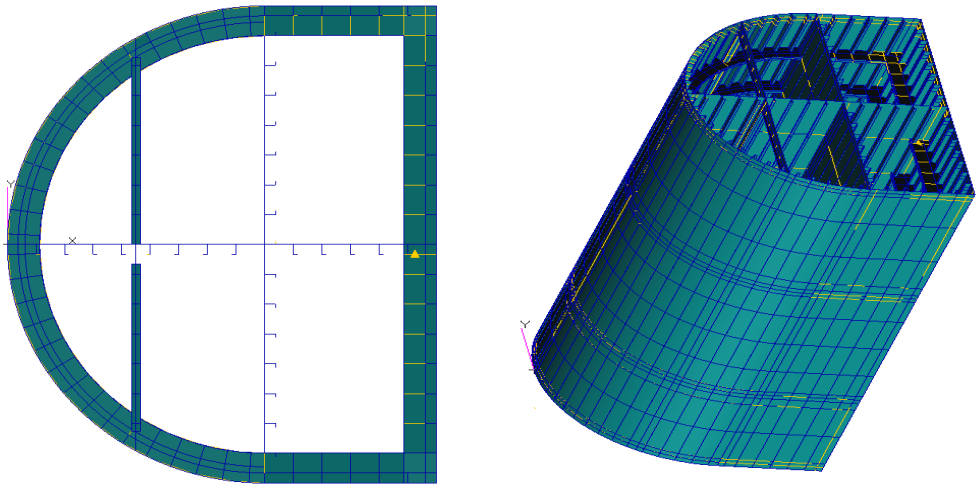

(a) Top view of step 3 (b) Arbitrary view of step 3

Figure 3.5: Step 3: Ring stiffner and outer plate modelling

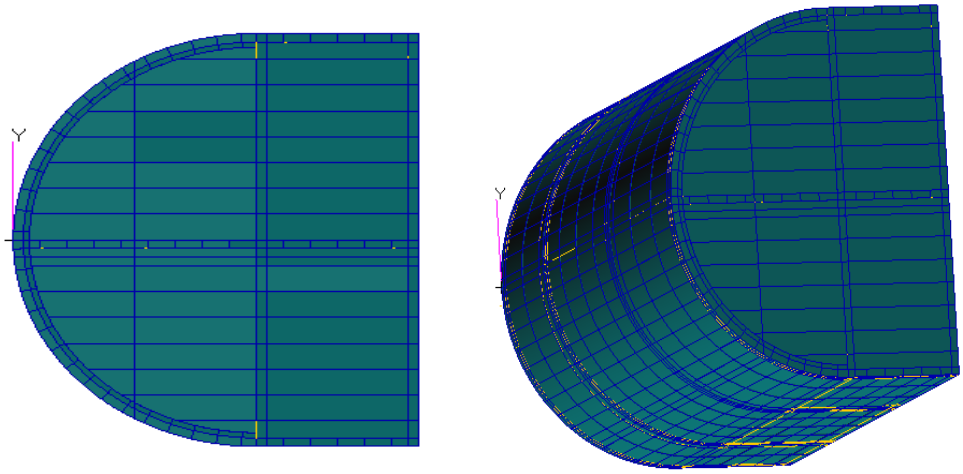

(a) Top view of step 4 (b) Arbitrary view of step 4

Figure 3.6: Step 4: Horizontal deck modelling

3.2 Mesh Generation

The principle of meshing is to make sure the mesh is continuous at the connection part of the model, i.e. the mesh at the connection part shares the same nodes. For example, the web elements should share the nodes with the plate and the flange, as Figure 3.7 shows.

An approximate mesh size of 75mm has been used to all the parts of the model.

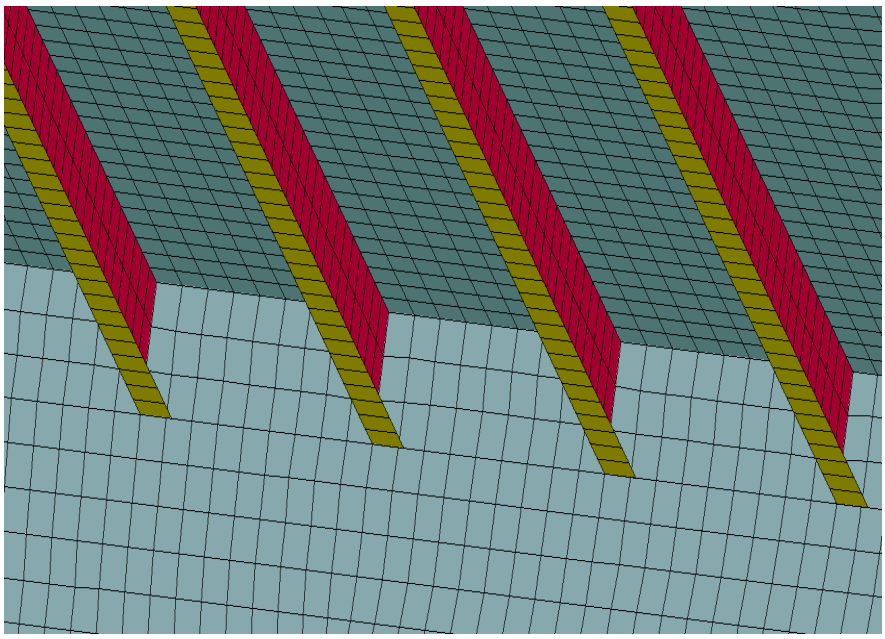

Figure 3.7: Mesh interaction between the longitudinal girder and the deck. The web elements share their nodes with the deck and the connected flange, but the flanges do not share nodes with the deck.

3.3 Material Model

Illustrated in the given figure, the material used for the pontoon is Grade NV A42, and the material for the ship is Grade NV A27.

The nonlinear material behavior can be defined in LS-DYNA material model by using number 041-050 by "USER DEFINED MATERIAL". The input parameters for user defined material model are the Youngs modulus, Poisson's ratio, Shear modulus, Bulk modulus, yield stress σ_Y, and the power law hardening parameters k and n, σ_{plat} and the critical strain ϵ_{cr}.

The Youngs modulus and Poisson's ratio were assumed to be 210 GPa and 0.3, respectively.

The relation between Youngs modulus E, Shear modulus G, Bulk modulus B and Poisson's ratio μ is given in Eq. 3.1 and Eq. 3.2.

$$G = \frac{E}{2(1+\mu)} \tag{3.1}$$

$$B = \frac{E}{3(1-2\mu)} \tag{3.2}$$

According to Eq. 3.1 and Eq. 3.2, the values of Shear modulus G, Bulk modulus B are obtained.

Yield stress for steel NV A42 and NV A27 are 420MPa and 270MPa respectively.

The relation between the stress and the strain is linear until the strain exceeds the yield strength, after which the relationship becomes nonlinear, shown in Figure 3.8.

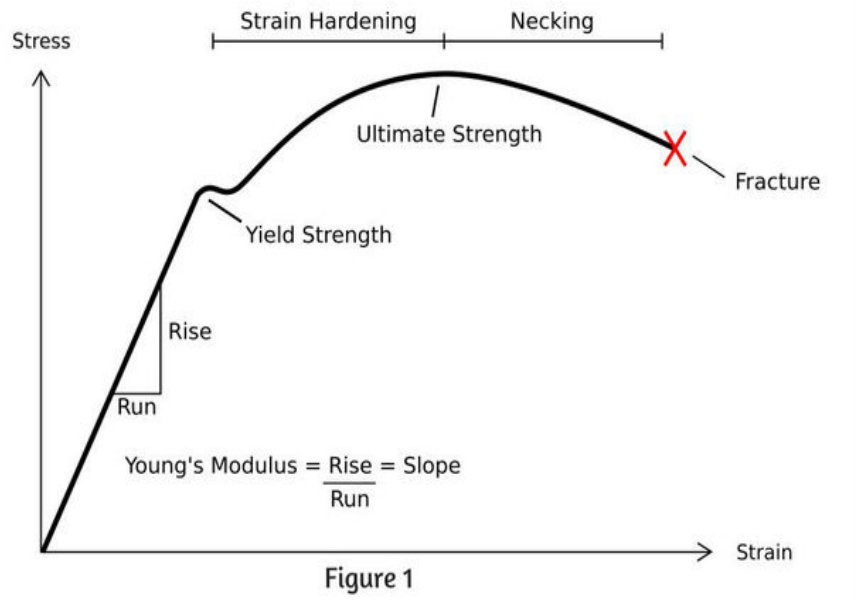

Figure 3.8: The relationship between the stress and strain

Power law parameters n and k can be calculated by Eq.3.3 and 3.4 based on the material requirements in DNV-OS-B101 (2016). Different power law parameters of different materials are shown in Table 3.1.

$$n = ln(1+\epsilon_{UTS}) \tag{3.3}$$

$$k = \sigma_{UTS}(e/n)^n \tag{3.4}$$

Grade	Min σ_Y	σ_{UTS}	$\epsilon_{fracture}$	$\epsilon_{necking}$	n	k
	[MPa]	[MPa]	[%]	[%]	-	[MPa]
NV A	235	400-520	22	18	0.166	636-827
NV A36	355	490-630	21	17	0.157	767-986
NV A46	460	570-720	19	15	0.140	863-1091

Table 3.1: Material parameters from DNV-OS-B101 (2016) with calculated power law parameters based on Eq. 3.3-3.4

According to Table 3.1, grade NV A42 is between NV A36 and NV A46 and NV A27 is between NV A and NV A36, the power law parameters n and k for Grade NV A42 and NV A27 can be calculated by assuming the relation is linear.

The critical strain ϵ_{cr} is mesh scaled in accordance with the relationship in Eq.3.5.

$$\epsilon_{cr} = n + (\epsilon_n - n)\frac{t_e}{l_e} \tag{3.5}$$

where n is the power low exponent, ϵ_n is the failure strain in terms of unaxial tension, l_e is the mesh length and t_e is the mesh thickness.

The input material data for ship NV A27 and pontoon NV A42 is shown in Table 3.2.

	E	μ	$Gmod$	$Bmod$	σ_Y	k	n	σ_{plat}	ϵ_{cr}
	[MPa]	-	[MPa]	[MPa]	[MPa]	[MPa]	-	[MPa]	-
Ship	2.1E11	0.3	7.96E10	1.73E11	2.75E8	8E8	0.161	0.005	0.16776
Pontoon	2.1E11	0.3	7.85E10	1.65E11	4.2E8	9.3E8	0.147	0.005	0.14725

Table 3.2: Material data for ship and pontoon

3.4 Analysis Setup in LS-DYNA

The ship model is a ship bow of a container ship, shown in Figure 3.9. There are several initial setups for the ship and the pontoon, which are:

1. Central collision between the ship bow and the pontoon, shown in figure 3.10.
2. Contact modelling. The contact modelling in LS-DYNA provides a way of treating interaction between disjoint parts. This is done by setting up different algorithms depending on what kind of the contact the user wants. In this thesis, Two types of contact modelling are used, which are contact single surface and contact surface to surface.
    - Contact single surface. The function of single surface contact is to make sure the structure itself will not pierce inside itself during collision.
    - Contact surface to surface. Two surface to surface contacts are made in this modelling. One is the forecastle to the pontoon, another one is the bulb to the pontoon.
3. The initial speed of the ship is $10 m/s$ in x-direction, another initial velocity is given to the rigid part of the ship by using *INITIAL VELOCITY GENERATION*, the function of it is to make sure the ship will not reduce the speed while experiencing the collision.
4. The boundary condition of the pontoon is indicated in figure 3.11, the white nodes of the pontoon are fixed in all degree of freedom.
5. The boundary condition of the ship bow is indicated in figure 3.12, the rigid part of the ship bow is only allowed to move in x-direction.

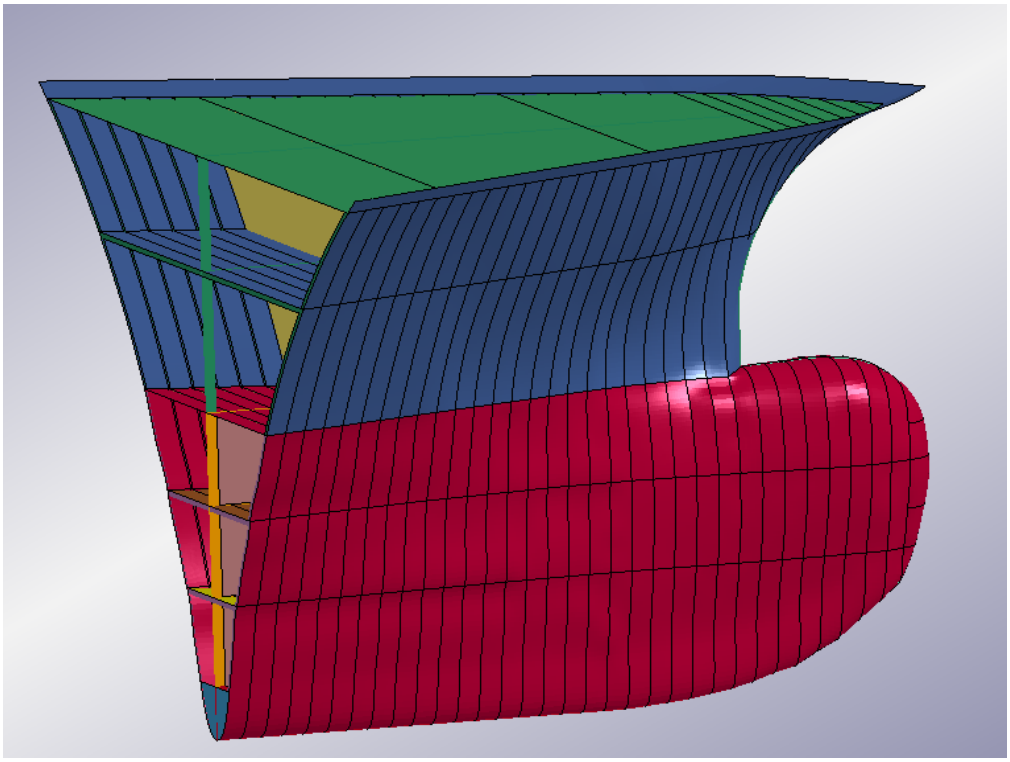

Figure 3.9: The model of ship bow

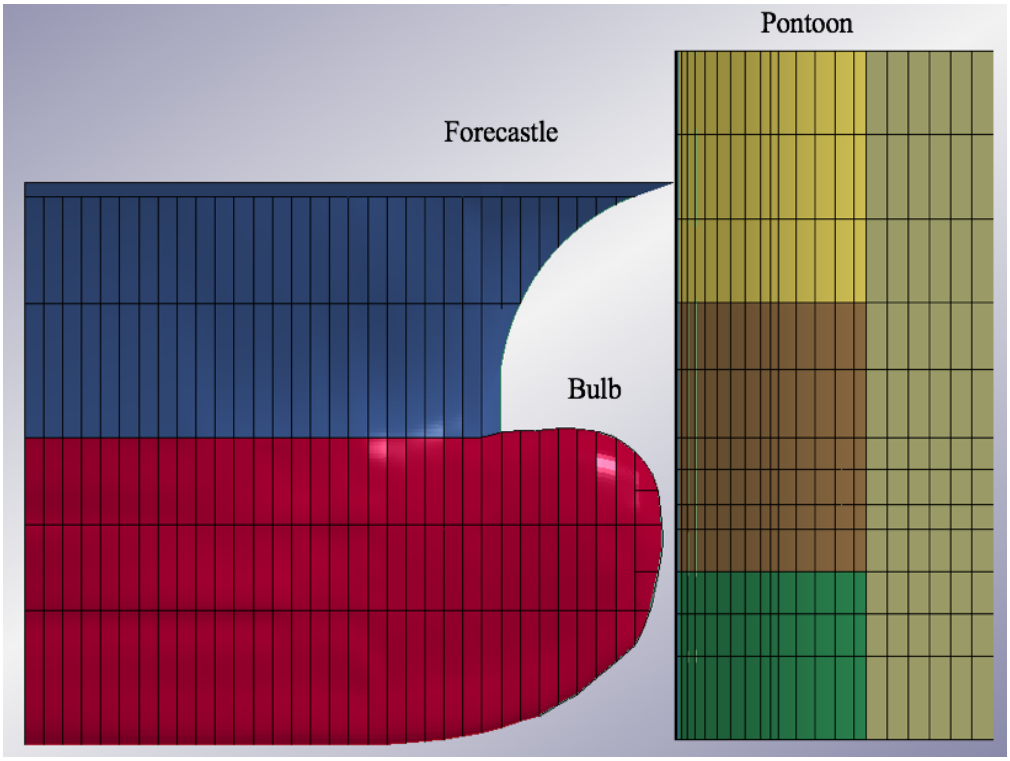

Figure 3.10: Central collision between the ship bow and pontoon

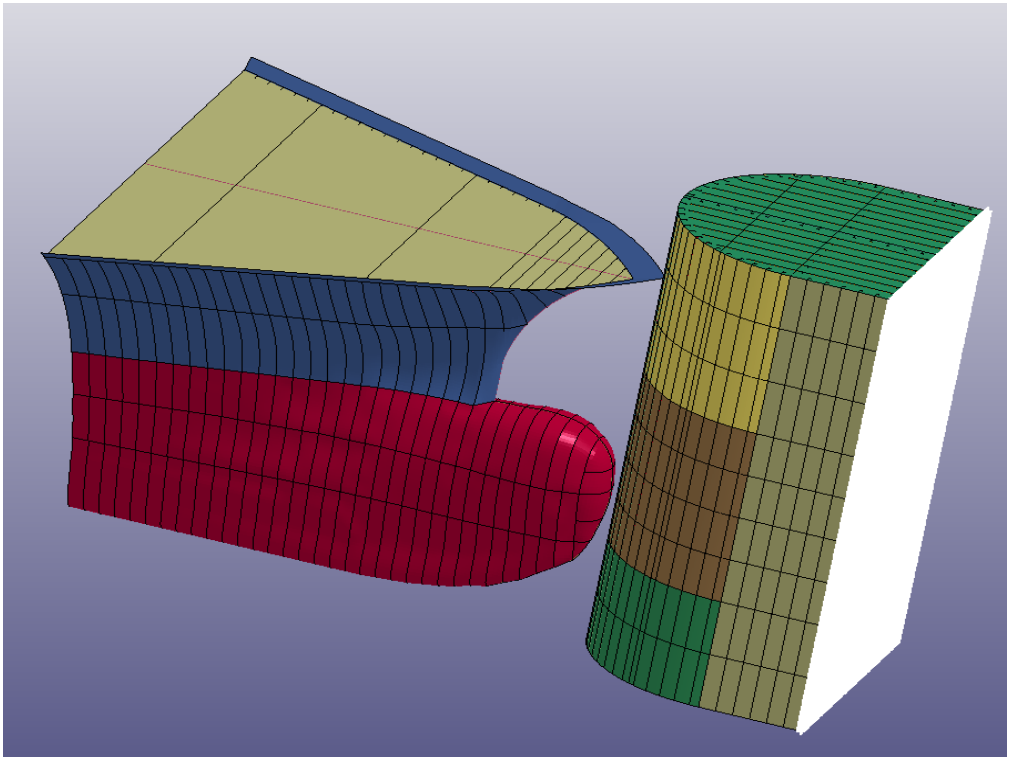

Figure 3.11: Boundary condition of the pontoon

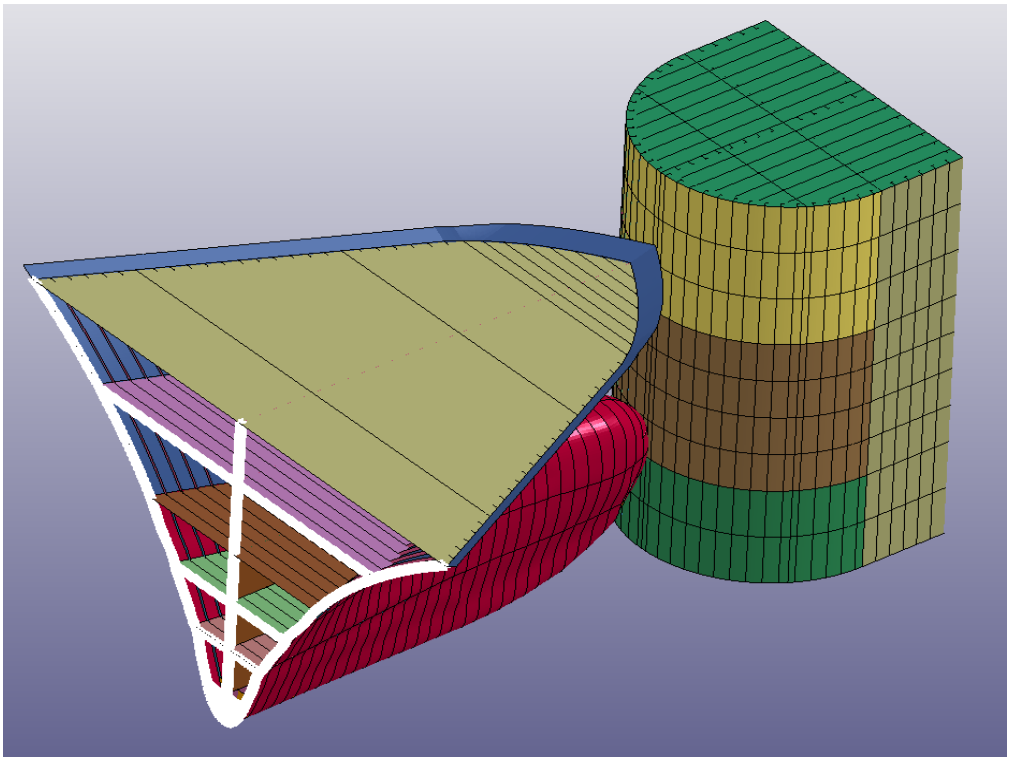

Figure 3.12: Boundary condition of the ship bow

3.5 Pontoon Steel Design

After simulation, it turns out that the strength of the original design is not strong enough, so it is suggested that the longitudinal girders that encounter directly to the ship should be strengthened by increasing their thickness, i.e. Case 2. However, it only helps a little by increasing the thickness of the longitudinal L profile girders and the thickness of the ring stiffeners, then the next step is to increase the thickness of the outer plate of the pontoon, i.e. Case 3. After obtaining the results from Case 3, it is suggested to add several ring stiffeners to strengthen the pontoon geometry.

The evolution of the properties of the geometry (from Case 1 to Case 3) is shown in Table 3.3.

	Girders	**Rings**	**Outer Plate**
Properties	L Profile(mm)	T Profile(mm)	mm
Case 1	250 × 90 × 9 × 13	750 × 250 × 12 × 15	14
Case 2	250 × 90 × 15 × 20	750 × 250 × 18 × 25	14
Case 3	250 × 90 × 15 × 20	750 × 250 × 18 × 25	20

Table 3.3: Different properties of the pontoon

Three additional ring stiffeners are added based on the position of the bulb. The original position of the ring stiffeners is shown in figure 3.13 while the added ring stiffeners are shown in figure 3.14. The aim of the added ring stiffeners is to resist the bulb, so the position is chosen to be in the middle of the original ring stiffeners, however, to make sure the mesh is continuous, one added ring stiffener is moved upwards to be closer to the deck inside the bulb to resist more collision force.

Under this condition, several cases with added ring stiffeners are investigated. The following cases have changed the thickness of the T profile ring stiffeners, the L profile longitudinal girders and the outer plate. The details of different cases are shown in table 3.4.

		Girders	**Rings**	**Outer Plate**
	Added ring stiffeners	L Profile(mm)	T Profile(mm)	mm
Case 4	✓	250 × 90 × 9 × 13	750 × 250 × 12 × 15	14
Case 5	✓	250 × 90 × 15 × 20	750 × 250 × 12 × 15	20
Case 6	✓	250 × 90 × 15 × 20	750 × 250 × 18 × 25	20

Table 3.4: Different properties of the pontoon under the condition of added ring stiffeners

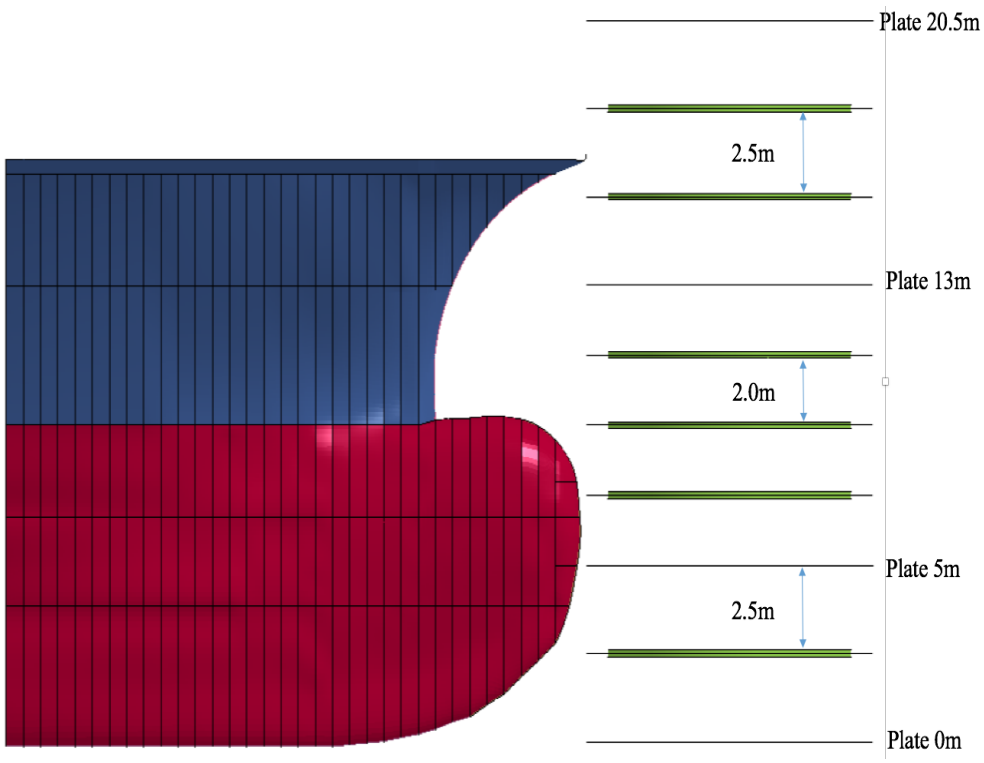

Figure 3.13: Original ring stiffeners position relative to ship bow

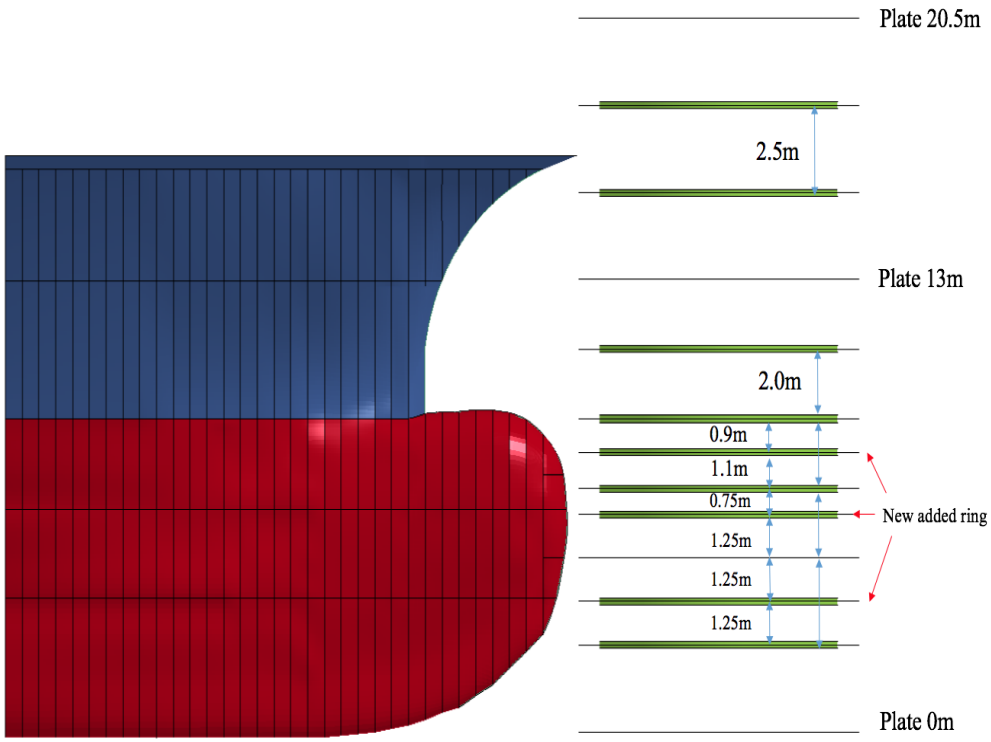

Figure 3.14: Added position of the ring stiffeners relative to ship bow

3.6 Results and Discussion

The global energy ratio of all cases are shown in table 3.5. The energy ratios in five cases are between 0.95-1, which proves the conservation of energy during the collision period.

	Case 1	**Case 2**	**Case 3**	**Case 4**	**Case 5**
Energy Ratio(Min Value)	0.962	0.95	0.966	0.993	0.998

Table 3.5: Global energy ratio of different cases

The results of the ship-pontoon collision are discussed as follows.

3.6.1 Cases with Original Geometry

In case 1, the base case, figure 3.15 and figure 3.16 show the ship bulb can easily penetrate the pontoon, however, the pontoon is strong enough to resist the forecastle.

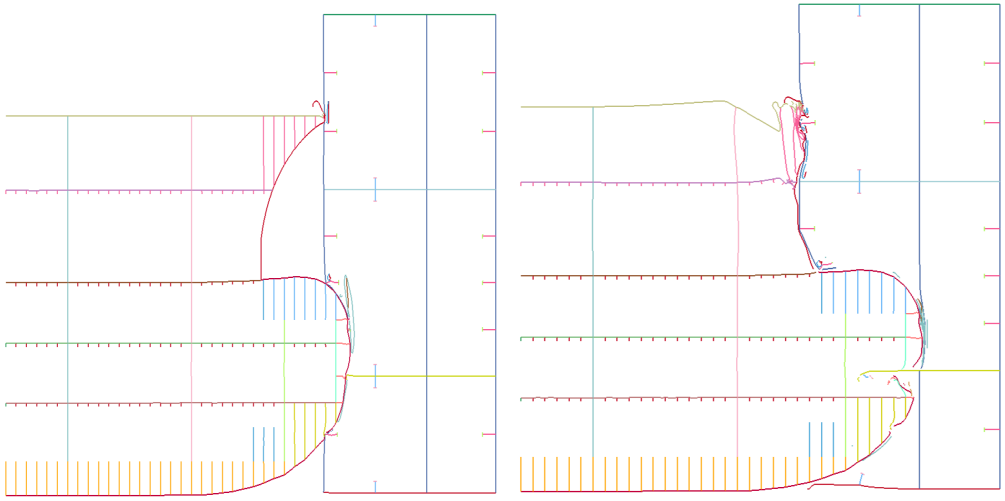

(a) Case 1, Longitudinal cut of the system at the beginning of the collision

(b) Case 1, Longitudinal cut of the system at the end of the collision

Figure 3.15: Case 1, Longitudinal cut of the system

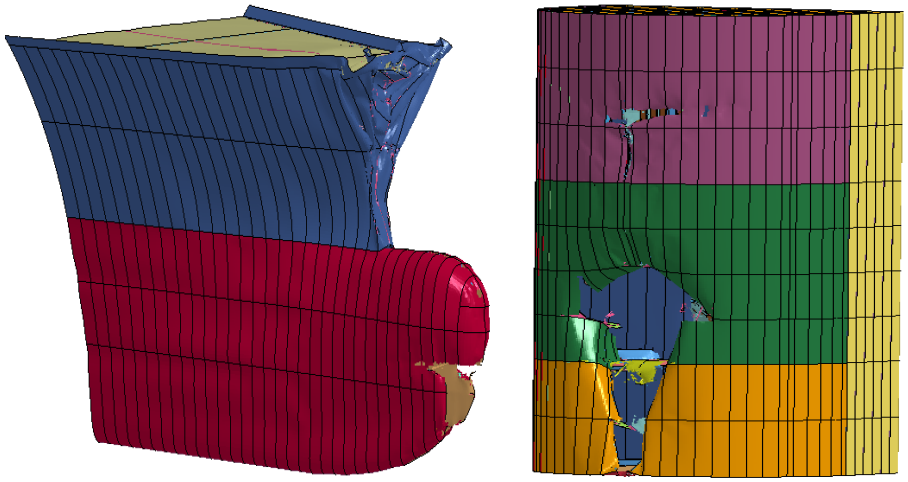

(a) Case 1, Ship shape after collision

(b) Case 1, Pontoon shape after collision

Figure 3.16: Case 1, General view after collision

In case 2, the thickness of the longitudinal girders and the rings have been increased, shown in table 3.3. The results from case 2 are shown in figure 3.17 and figure 3.18. It appears that the

pontoon is still not strong to resist the ship bulb.

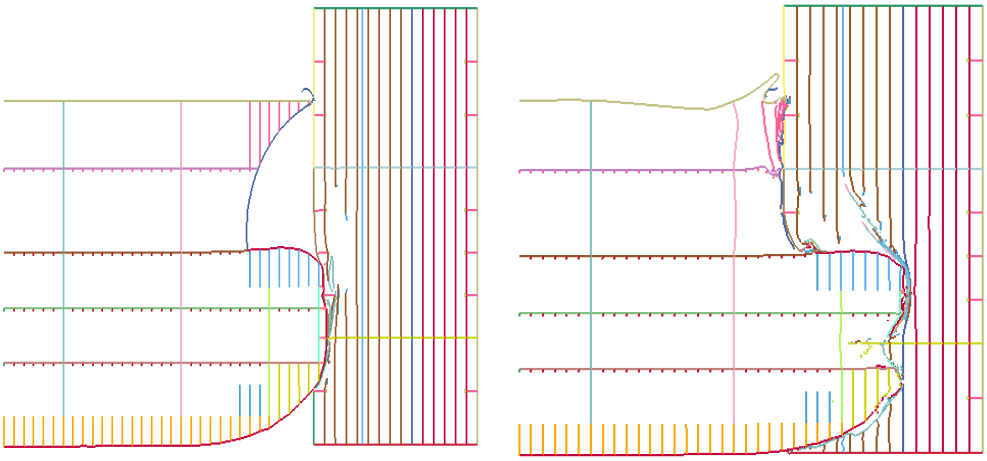

(a) Case 2, Longitudinal cut of the system at the beginning of the collision

(b) Case 2, Longitudinal cut of the system at the end of the collision

Figure 3.17: Case 2, Longitudinal cut of the system

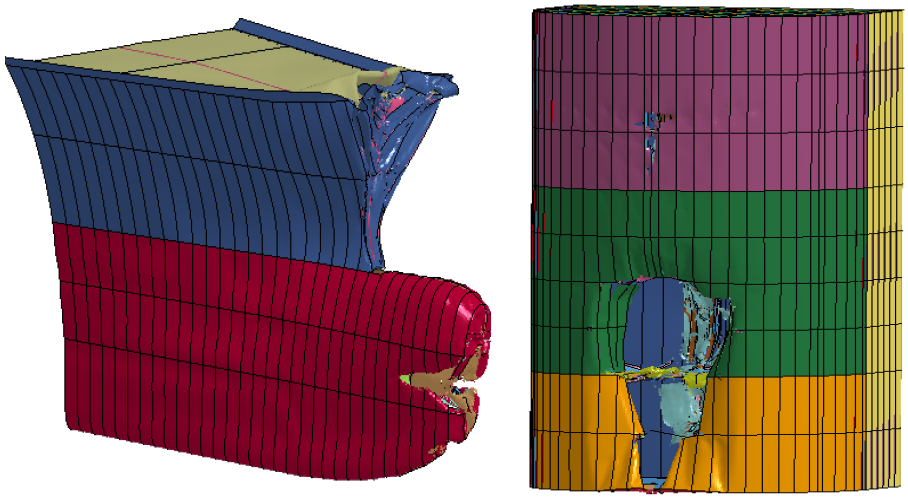

(a) Case 2, Ship shape after collision

(b) Case 2, Pontoon shape after collision

Figure 3.18: Case 2, General view after collision

In case 3, not only the thickness of the longitudinal girders and the rings are increased, the thickness of the outer plate is increased from 14mm to 20mm. The figure 3.19 and 3.19 illustrate the collision results of case 3.

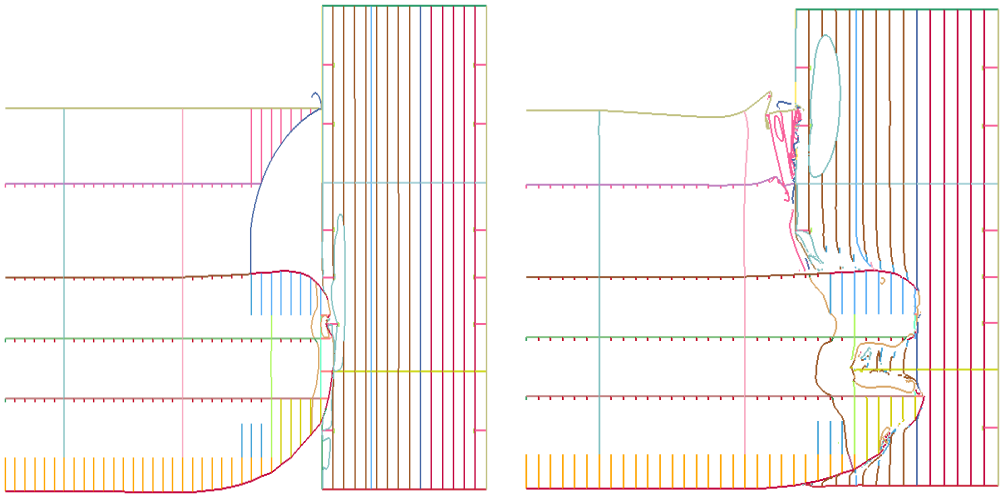

(a) Case 3, Ship shape after collision (b) Case 3, Pontoon shape after collision

Figure 3.19: Case 3, Longitudinal cut of the system

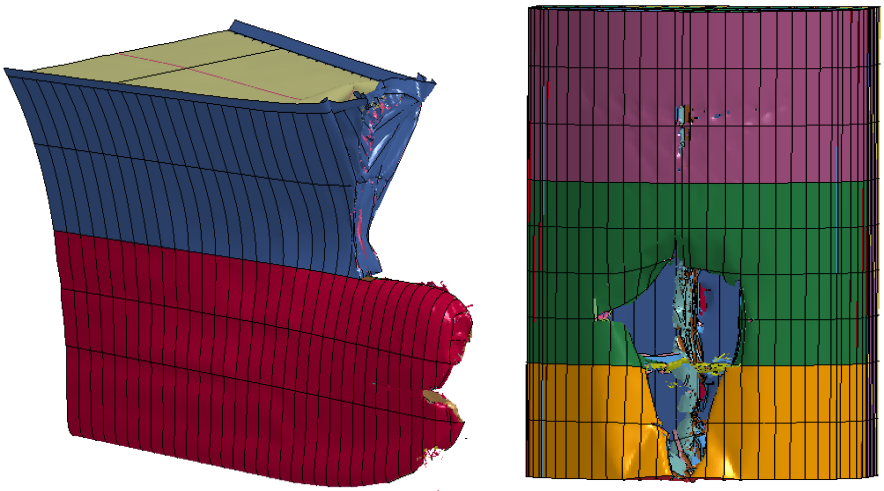

(a) Case 3, Ship shape after collision (b) Case 3, Pontoon shape after collision

Figure 3.20: Case 3, General view after collision

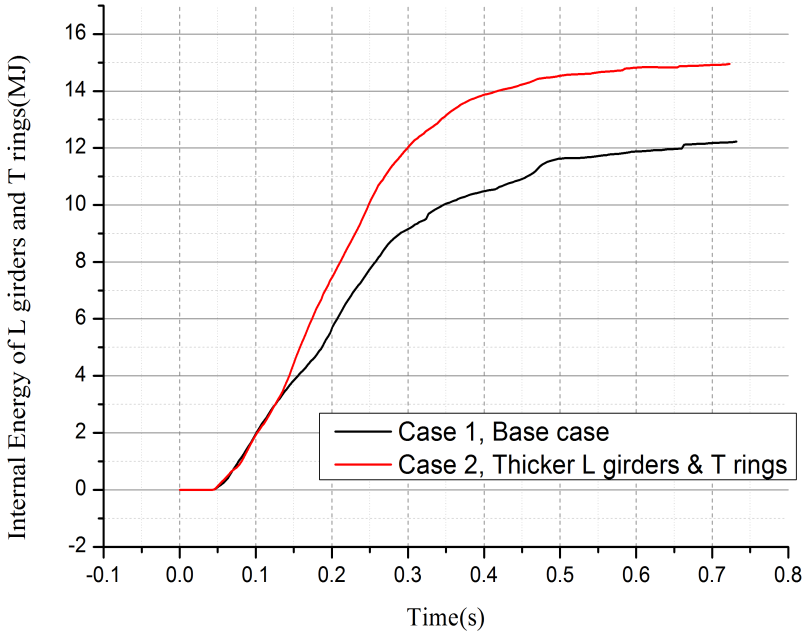

Figure 3.21: The internal energy of the L profile girders and T profile rings in case 1 and case 2

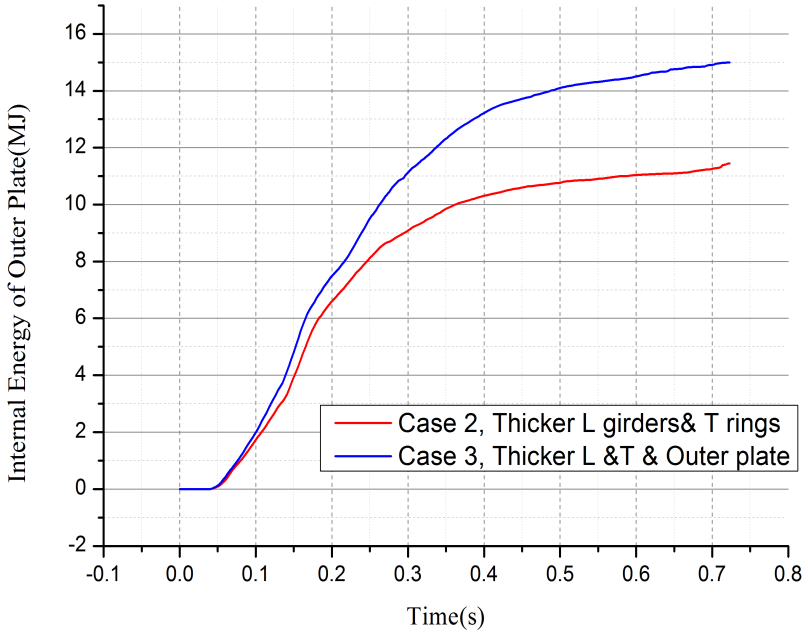

Figure 3.22: The internal energy of the outer plate in case 2 and case 3

Case 2 has a thicker L profile girders and T profile ring stiffeners compared to the base case, it is interesting to see how the internal energy of L profile girders and T profile ring stiffeners changes in the two cases. Figure 3.21 shows the internal energy difference in case 1 and case 2, the internal energy of L profile girders and T profile ring stiffeners in case 2 is larger than that in case 1, which means the thickened girders and rings absorb more energy during the collision.

Compared with case 2, case 3 has a thicker outer plate. The comparison of the internal energy of the outer plate in case 2 and case 3 is done in figure 3.22. It is apparent that the 20mm outer plate in case 3 absorbs more energy than the 14mm outer plate in case 2.

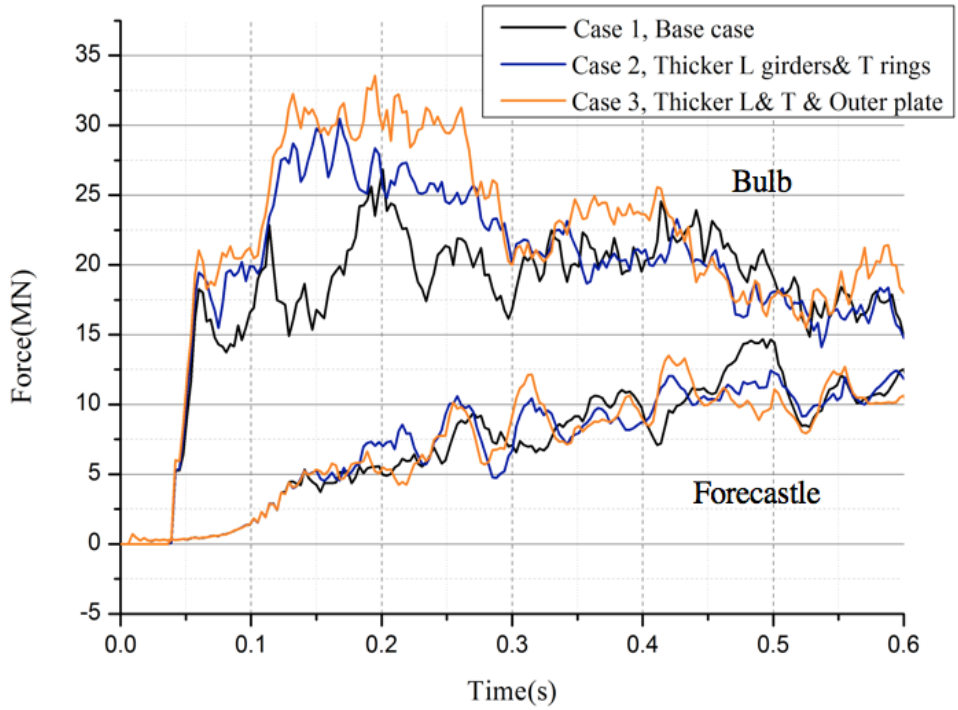

Figure 3.23: Force curve comparison between case 1, case 2 and case 3. The upper 3 curves represent the force of the bulb in three cases while the lower 3 curves represent the force of the forecastle.

From figure 3.15 to figure **??**, it can be seen that the design of pontoon in these three cases are not strong enough to resist the ship collision.

The resultant forces of case 1, case 2 and case 3 are shown in figure 3.23. It can be seen that the force of the forecastle in these three cases does not fluctuate so much, because in case 1 the

forecastle breaks easily which means the strength of the pontoon is enough for the forecastle and in case 2 and case 3 the pontoon structure is strengthened, then the forecastle would break easier than that in case 1.

In terms of the bulb, the most attractive difference between case 1 and case 2 occurs around 0.15s. In case 1, the force has a sudden drop while the force in case 2 increases. The reason can be, in case 1, at 0.15s the pontoon breaks in a large scale, so the contact area between the bulb and the pontoon decreases so that the contact force decreases. As in case 2, the L profile girders and T profile rings are strengthened, so at 0.15s, the damage of the pontoon does not happen so quickly, as a result, the contact force has increased. After around 1s, the force decreases approaching to that in case 1, meaning the damage of the pontoon begins to increase. The same situation occurs in case 3. In case 3, not only the L profile girders and the T profile rings have been strengthened, but also the thickness of the outer plate is increased from 14mm to 20mm. The resultant force of of the bulb in case 3 is the largest in the beginning 0.4 seconds due to the reinforcement of the plate, after which the force starts to decrease to the same level as that in case 1 and case 2. This means increasing the thickness has affected the collision condition for the bulb.

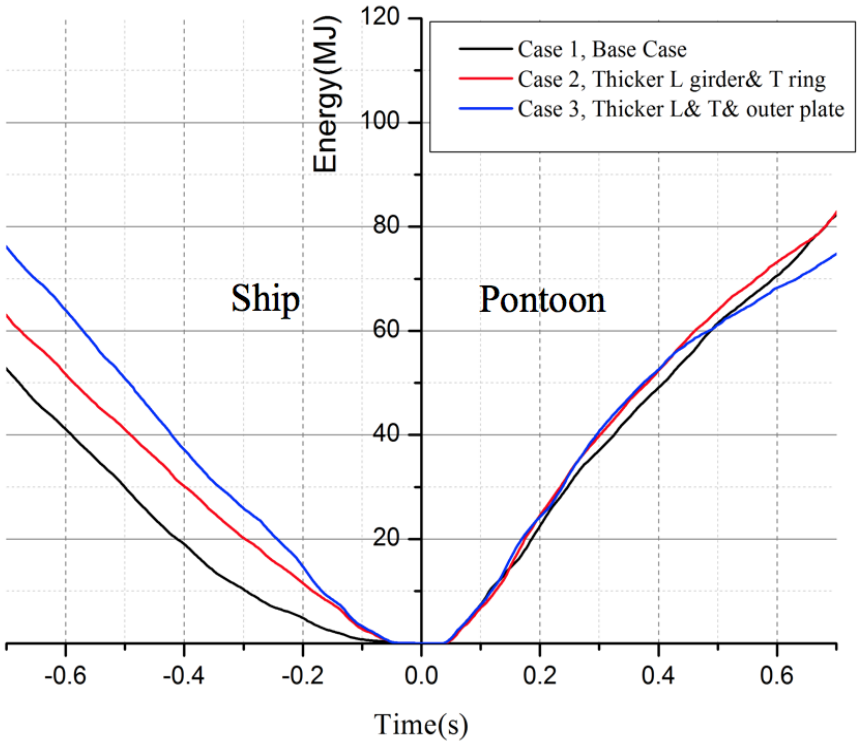

Figure 3.24: Energy dissipation between ship bow and pontoon in Case 1, Case 2 and Case 3

Figure 3.24 shows how the energy between ship bow and the pontoon changes in different cases. For the ship, from the base case to case 3, the total internal energy has increased due to the increased thickness of the girder, rings and the outer plate, the damage of the ship is getting larger. However, the energy of the pontoon barely indicates difference in the three cases. The main reason is that the damage of the pontoon is huge in each case and the bulb penetrates the pontoon easily, so the energy of the pontoon does not change so much even in case 2 and case 3.

3.6.2 Cases with Added Ring Stiffeners

Case 4, case 5 and case 6 are under the condition that three more ring stiffeners are added to the pontoon, the results are shown as follows.

On the basis of case 4, case 5 has thicker L profile girders and outer plate and case 6 has thicker L profile girders, T profile rings stiffeners and outer plate.

Figure 3.25 shows the contact force between the bulb-pontoon and the forecastle-pontoon. The contact force of the bulb is much larger than the contact force of the forecastle. In terms of the contact force of the bulb, the force of case 4, case 5 and case 6 are higher than that in case 1, which means the strengthened rings have a positive contribution for resisting the ship.

It is indicated that in the figure 3.25 the force in case 6 has the largest average value. The only difference between case 5 and case 6 is that case 6 has a thicker outer plane than case 5. In the first 0.3s, the force in case 5 is lower than the force in case 6, but not in a large degree. However, after 0.3s, the force in case 5 (blue line) starts to decrease and the force in case 6 stays at the same level, which means the structure in case 6 does not break so much, the contact area is similar to that at the beginning of the collision.

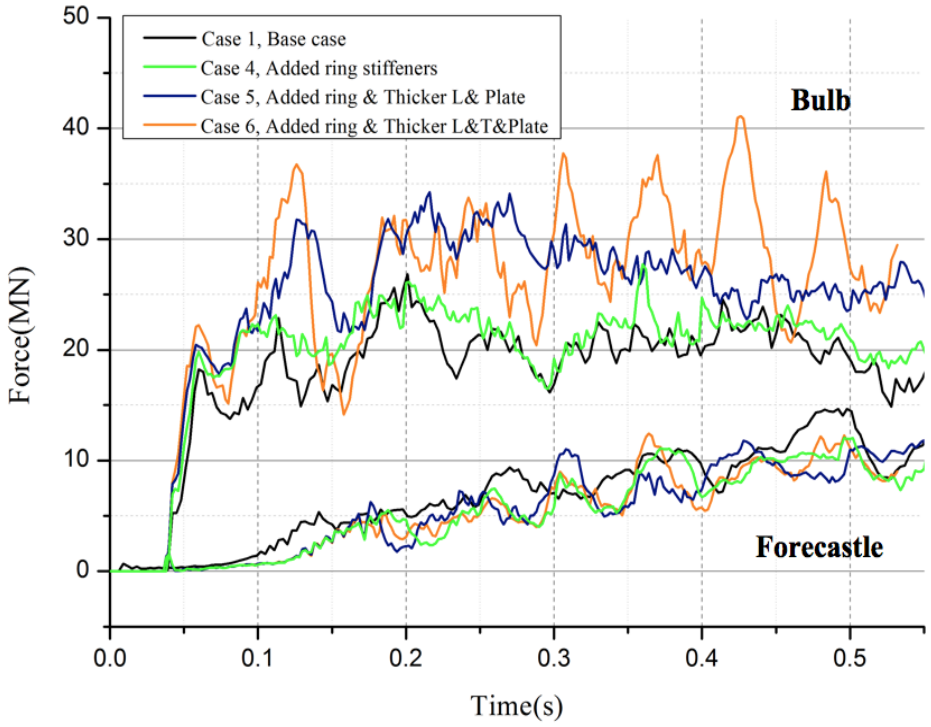

Figure 3.25: Force curve comparison between case 1, case 4, case 5 and case 6. The upper 4 curves represent the force of the bulb in three cases while the lower 4 curves represent the force of the forecastle.

Figure 3.26 shows the energy dissipation between the ship and the pontoon in these 4 cases, including case 1, the base case. In case 4, even though more rings are added to the pontoon and the internal energy of the ship is increased, the energy of the pontoon is still in the same level

as that in case 1. It can be seen clearly in case 5 and case 6, the pontoon energy has decreased in a relatively large scale compared to the base case. In case 6, the pontoon internal energy is reduced to around 12MJ, which means the damage of the pontoon is in an acceptable range. This is also seen in figure 3.27b. From these 3 cases, it can be concluded that the increased thickness of the girders, rings and outer plates are essential to resist the collision of the ship.

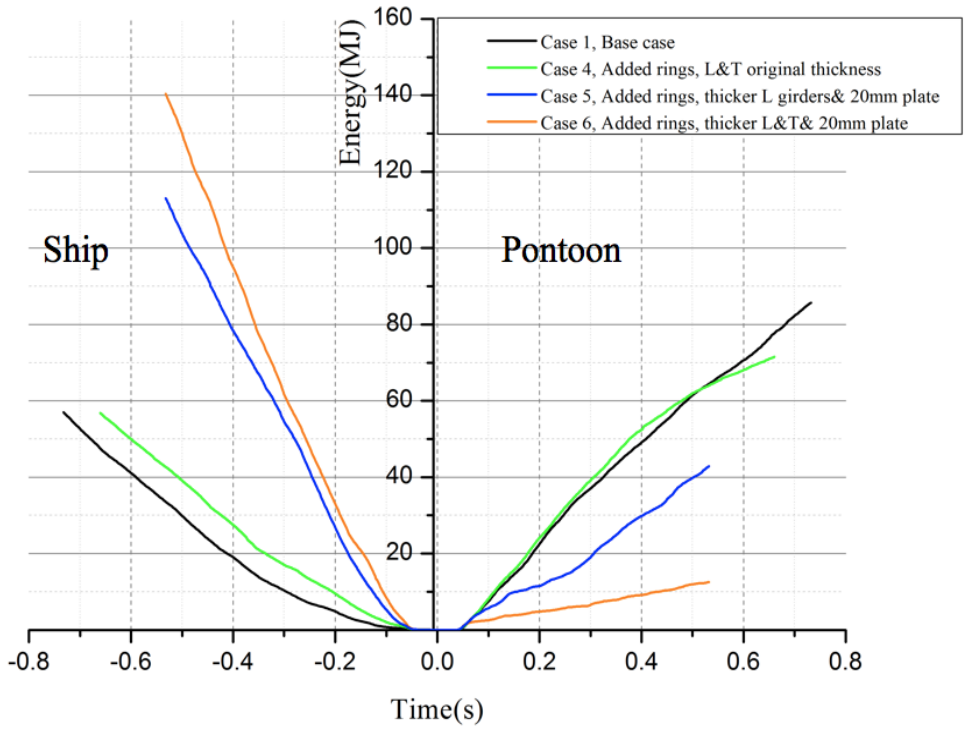

Figure 3.26: Energy dissipation between ship bow and pontoon in Case 1, Case 4, Case 5 and Case 6

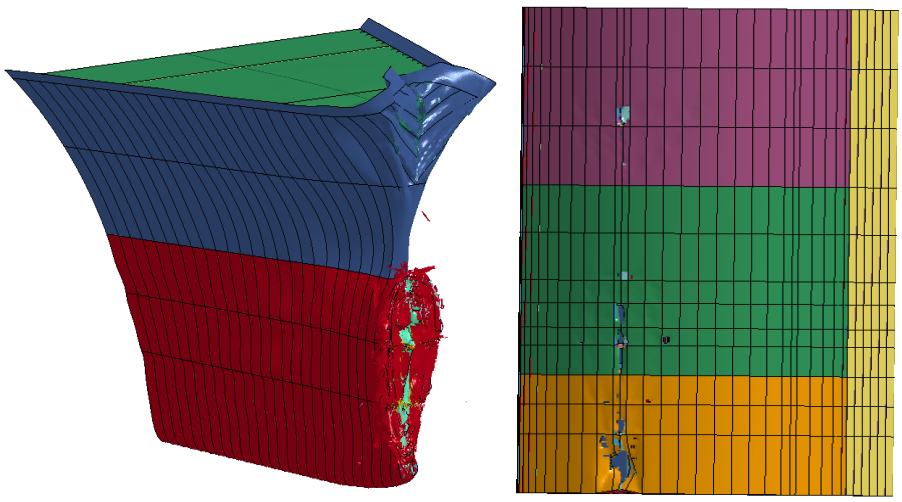

(a) Case 6, Ship shape after collision (b) Case 6, Pontoon shape after collision

Figure 3.27: Case 6, General view after collision

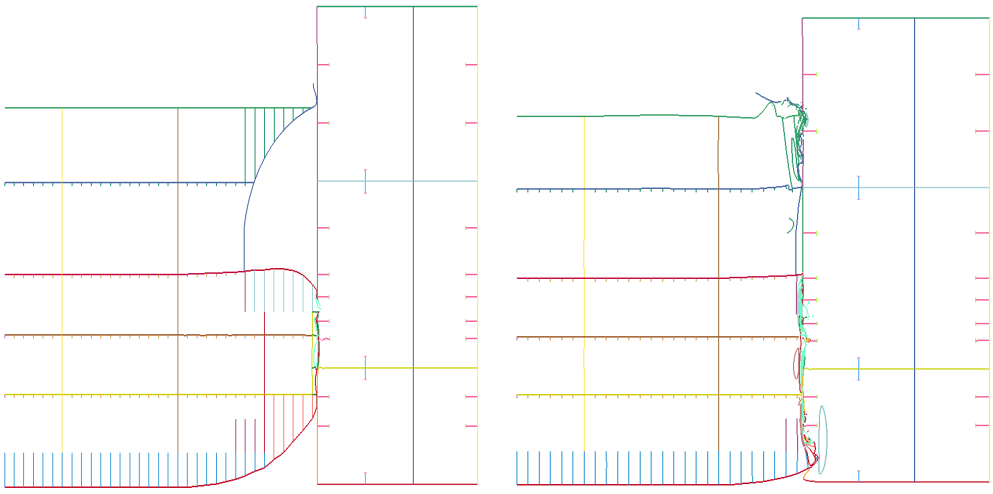

(a) Case 6, Longitudinal cut of the system at the beginning of the collision (b) Case 6, Longitudinal cut of the system at the end of the collision

Figure 3.28: Case 6, General view after collision

3.6.3 The Proposed Safe Pontoon Design

Case 6 has the strongest strength since it has added ring stiffeners, the thickness of the L girders, T ring stiffeners and the outer plate is increased as well. Figure 3.27 shows the collision condition in case 6. It can be seen that the ship bow is totally crushed by the pontoon and the damage of

the pontoon is relatively small compared to the condition in case 1.

Figure 3.28 shows the longitudinal cut of the whole system at the beginning and the end of the collision. It can be seen that the ship can not penetrate into the pontoon easily, so the pontoon is strong enough to resist the collision.

Case 6 can be regarded as a safe design of the pontoon, the proposed safe design is shown in table 3.6.

		Girders	**Rings**	**Outer Plate**
	Added ring stiffeners	L Profile(mm)	T Profile(mm)	mm
Case 6	✓	250 × 90 × 15 × 20	750 × 250 × 18 × 25	20

Table 3.6: The proposed safe design of pontoon

3.6.4 Discussion

The material used for the pontoon is high strength steel NV A42, the parameters such as the shear modulus, bulk modulus and power law parameters are calculated by the author according to DNV-OS-B101 (2016) and Storheim (2016). The material input is close to practical engineering material since the non-linear parameters have been taken into consideration. It is a conservative design that the entire pontoon is made of the high strength steel, for example, the longitudinal girders and the vertical plates that are not close to the collision part so they contribute little to the force deformation curve. It is suggested that further investigation can be conducted by using normal steel applied to these parts.

It is obvious that in all the 6 cases, the force obtained from bulb is around twice than the force of the forecastle. For forecastle, the force in these 6 cases does not change so much since in the original design the pontoon has enough strength to resist the collision of forecastle. For the ship bulb, the force does not have a significant change from case 1 to case 4, however, in case 5 and 6, the bulb force has increased, from average 20MN(case 1) to 25MN(case 5) and 30MN(case 6). Combined with the results in figure 3.26, one can see the energy that the pontoon absorbed in case 5 and case 6 has decreased from 82MJ(case 1) to 42MJ(case 5) and 12MJ(case 6). With the

small internal energy of the pontoon, the design in case 6 can be regarded as a relatively safe design. It is suggested that, in reality, the thickness of ring near the forecastle part does not need to be increased since the original design case can resist the collision, otherwise it will be a waste of material.

The force deformation curve obtained from case 6 will be used in the global analysis of ship bridge collision in USFOS. The curve is considered practical enough since no global buckling mode is observed during the collision process.

Chapter 4

Global Analysis of the Bridge

4.1 Bjørnefjorden Bridge Structure

A brief description of the Bjørnefjorden bridge will be presented in this chapter, more detailed modelling can be referred to Wang (2016).

A general view of the floating bridge is shown in figure 4.1. The bridge is a symmetric structure supported by 20 pontoons with two towers in the middle. The towers are also connected with the bridge by the cables. The total length of the bridge is 4198 meters, the height of the tower is 155 meters from sea level. The entire bridge is modelled in USFOS. The coordinate of the nodes is calculated based on the geometry of the bridge, the Matlab transcript for the coordinate calculation is attached in Appendix A. The frequent used definitions related to the bridge are shown in figure 4.2.

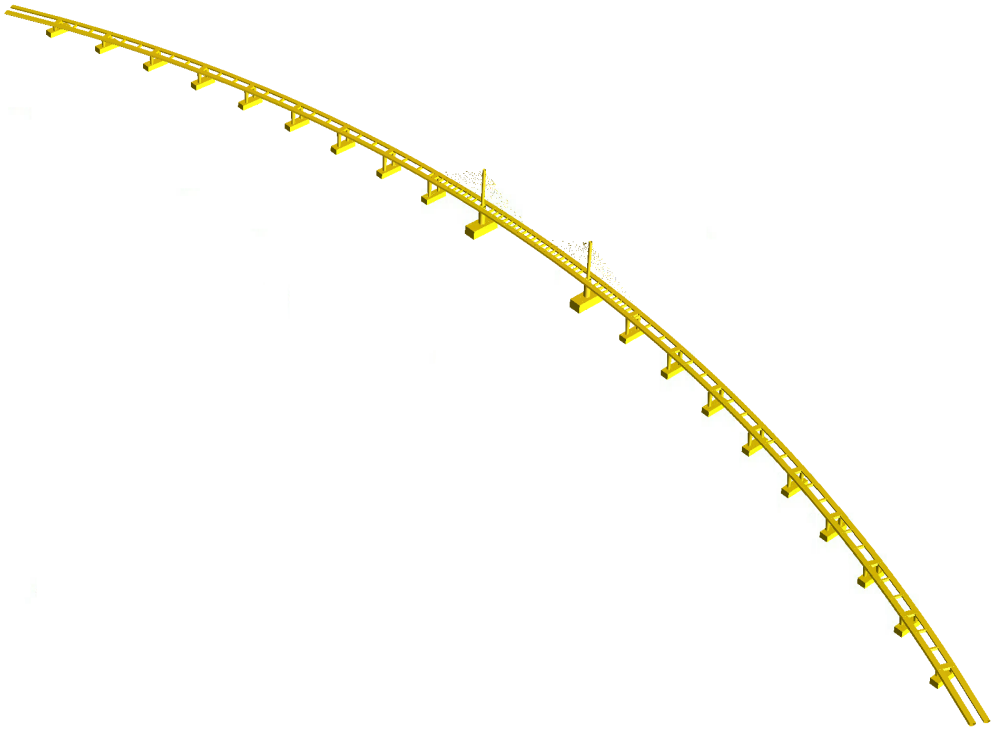

Figure 4.1: A general view of the Bjørnefjorden bridge

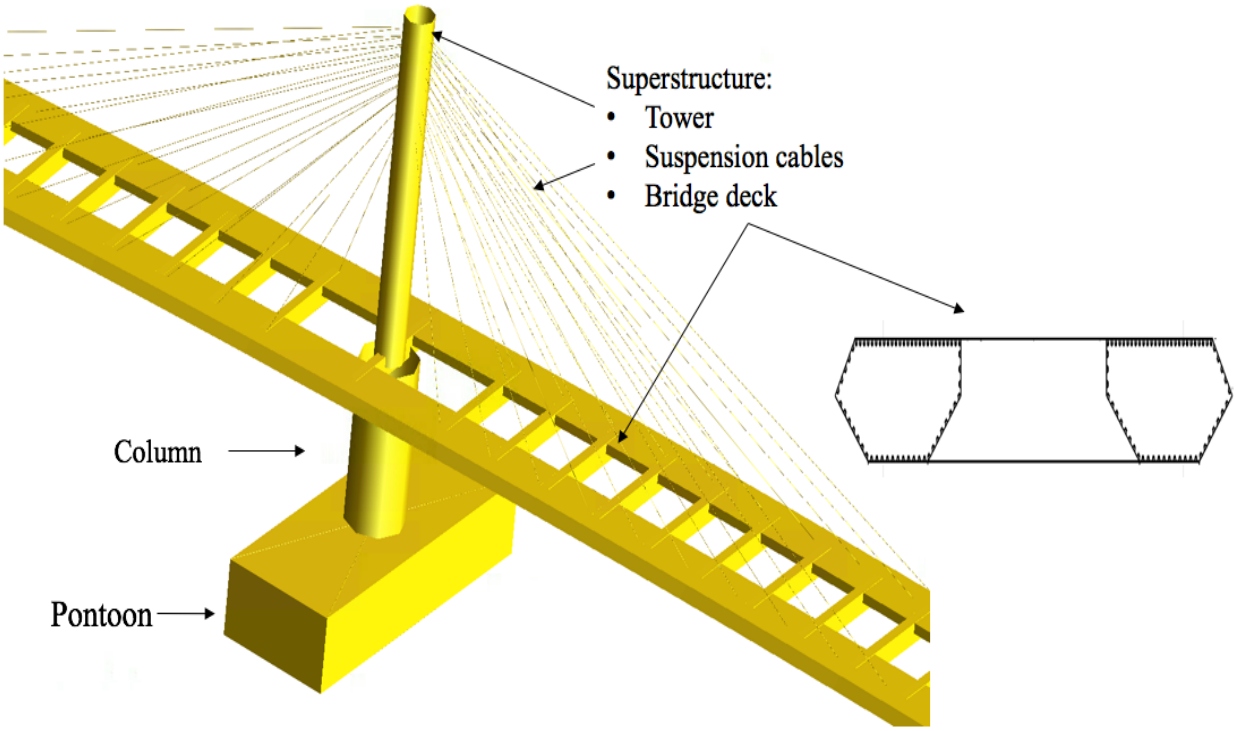

Figure 4.2: Bjørnefjorden bridge structure definitions

4.2 Finite Element Model in USFOS

4.2.1 Bridge Girder

The bridge has two pathways for the traffic, the two girders are connected by the beams. The geometry of the cross section of the girder is shown in figure 4.3. In the drawing, the information given about the girder thickness is from $30mm$ to $50mm$, in the modelling, the average thickness $45mm$ is used. In USFOS, the command GENBEAM is used to define the basic structural properties of the girder, including the cross section area, the moment of inertia, plastic modulus and shear area. To have a comfortable look of the bridge girder in USFOS, the command SurfArbit is used.

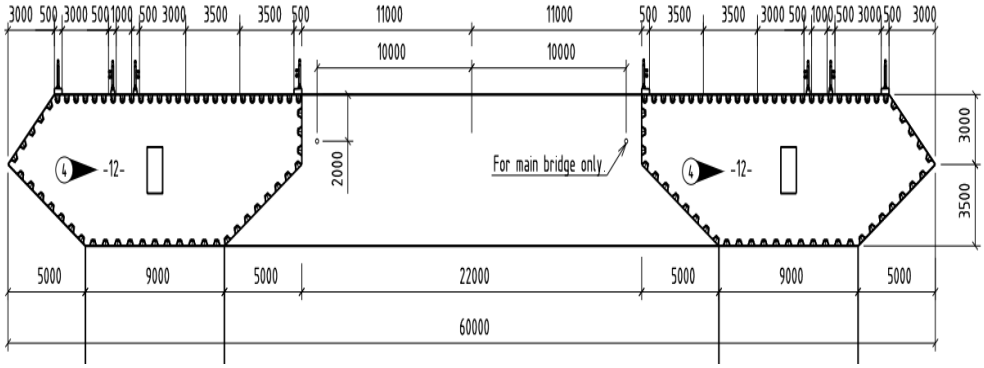

Figure 4.3: Bridge girder cross section

Moment of Inertia

The cross section area and the moment of inertia about y-axis and z-axis for one girder are calculated by Auto CAD. The moment of inertia is calculated regarding to the axis of itself. The result is shown in table 4.1.

$Area(m^2)$	$I_y(m^4)$	$I_z(m^4)$
1.8389	13.537	70.717

Table 4.1: Structural properties of the bridge girder

Referring to Ole Eldegard's calculation(Eldegard (2016)), in his case the two bridge girders are

considered as one, the values are as follows, the area is $4m^2$, I_y is $26.96m^4$, I_z is $1617.24m^4$. To make sure the properties are not wrong, results from the two methods are compared. Apparently, the area from second method ($4m^2$) is around twice larger than the result from the first method ($1.8389m^2$), which is reasonable. To check the moment of inertia, the parallel axis theorem is used.

$$I'_y = I_y + S * ly^2 \tag{4.1}$$

$$I'_z = I_z + S * lz^2 \tag{4.2}$$

where l_y and l_z are the distance from the local coordinate to the global coordinate of y-axis and z-axis respectively. S is the corss section area of one girder, i.e $1.8389m^2$. After inserting the numbers into the equations, the results from the two methods match, meaning the calculation of the area and the moment of inertia are correct.

Plastic Modulus

The plastic section modulus needs to be specified when a limited plastic behavior is acceptable and the formulae is given by Eq. 4.3.

$$Z_p = A_C y_C + A_T y_T \tag{4.3}$$

where $A_{C/T}$ is the compressible/torsional area and $y_{C/T}$ is the distance of each area to the plastic neutral axis (PNA). Different from neutral axis, PNA is defined as the axis that equally spits the cross section for most typical sections with constant yielding stress (Moan (2003)). Therefore the local z-PMA is chosen as the vertical middle line because of symmetry and local y-PMA is set as roughly the horizontal central line as well for simplicity. Each edge is treated as a rectangular for calculation and the results are approximately $Z_{py} = 4.68m^3$ and $Z_{pz} = 37.98m^3$.

4.2.2 Pontoon

The bridge is supported by 20 pontoons including 2 middle pontoons and 18 side pontoons. The pontoons are made of weight concrete, assuming the density is $2500kg/m^3$. The function of the pontoons is to provide the bouncy for the bridge, so they are modeled as buoyancy elements.

Figure 4.4 shows the geometry of the middle pontoon.

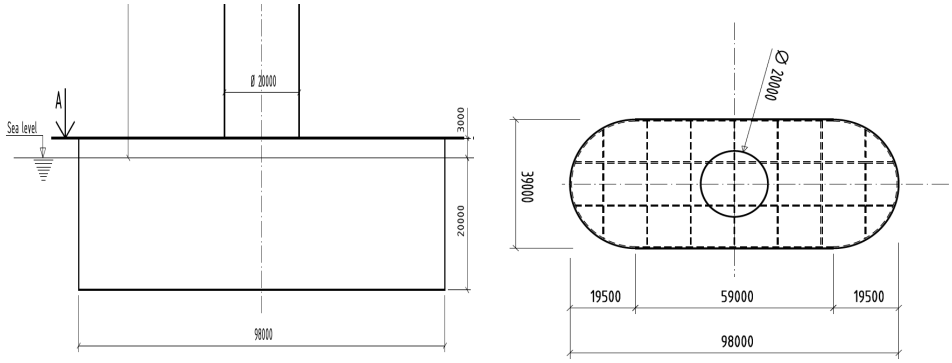

(a) Side view of the middle pontoon (b) Top view of the middle pontoon

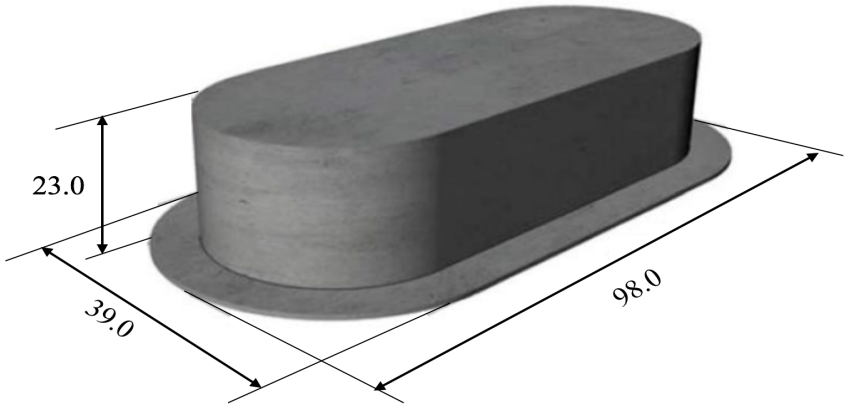

(c) 3D view of middle pontoon

Figure 4.4: Middle pontoon geometry

The pontoons are simplified as a rectangular boxes with the geometry configuration shown in table 4.2.

	Length	**Width**	**Height**	**Draught**
	m	m	m	m
Middle pontoons	98	39	23	20
Side pontoons	79	26	14.5	11.5

Table 4.2: Geometry of the pontoons

The material of the pontoons are assumed to be hyperelastic material, it is defined by using the command HYPELAST with two points describing the force-displacement curve.

To have an equilibrium condition of the bridge, it is important to calculate the ballast of the pontoons. By subtracting the weight that the pontoon holds from the buoyancy of each pontoon, the ballast of each pontoon is obtained. For example, for a side pontoon, the ballast weight equals to the buoyancy of the side pontoon minus the sum weight of the main bridge of 186m, the two beams in this section and the two columns on the pontoon. The ballast conditions of different pontoons are shown in table 4.3. This is a very ideal condition, during modelling, the values of the nodemass need to be adjusted for many times by doing dynamic analysis of the bridge.

Pontoon	**Ballast(kg)**
Middle Pontoons	$4.3E7$
Side Pontoons	$1.3E7$

Table 4.3: Ballast of the pontoons

This method is a very rough estimation of the ballast, because some weight of the bridge are taken by the ends of the bridge abutments. For the 2 middle pontoons, it is very difficult to estimate accurately how much weight from the cables that is held by the pontoons. In addition, one can not say that the weight of the section upwards one pontoon is carried exactly by the corresponding pontoon, the weight maybe carried by other pontoons as well. In this way, the stability of the bridge needs to be checked until the equilibrium condition is reached.

In USFOS, the pontoons are modelled using a special buoyancy element. The stiffness of the pontoon are guaranteed by using one node spring connecting with the pontoon on water surface. The springs have the stiffness in heave, roll and pitch.

Since a large part of the pontoons is submerged in the water, the hydrodynamic effect of the added mass needs to be considered.

The added mass of the pontoons can be calculated by using the added mass coefficient given in the *Curved Bridge-Navigation Channel In South*, see figure 4.5.

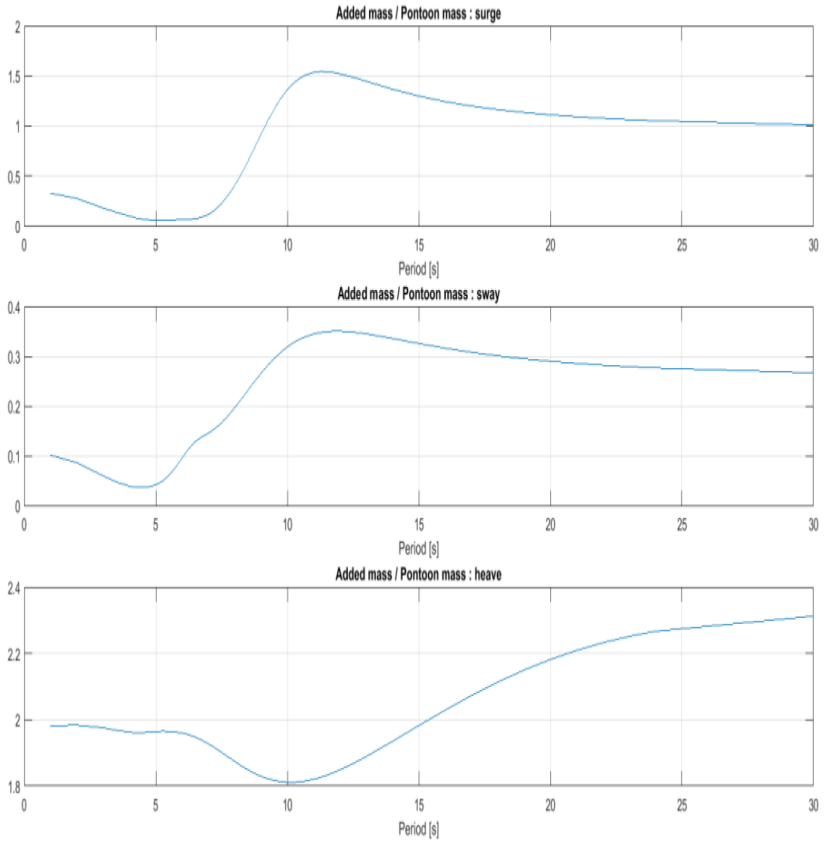

Figure 4.5: Added mass coefficients. Reprinted from COWI (2016)

Since the added mass needs to be added on the virtual elements on the pontoons, one thing needs to be paid attention to is the different definition of the axis of the beam element in USFOS and the local axis of the pontoons in terms of the surge, sway and heave.

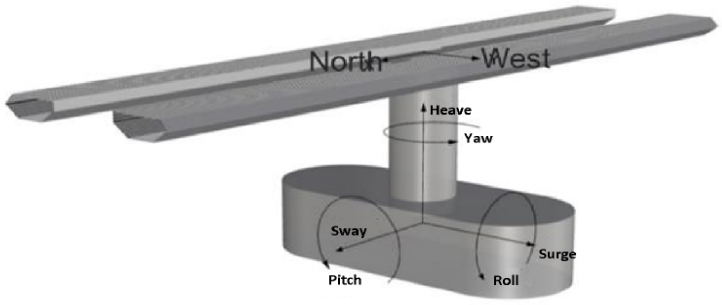

Figure 4.6: Sway Surge and Heave defined in pontoon. Reprinted from COWI (2016)

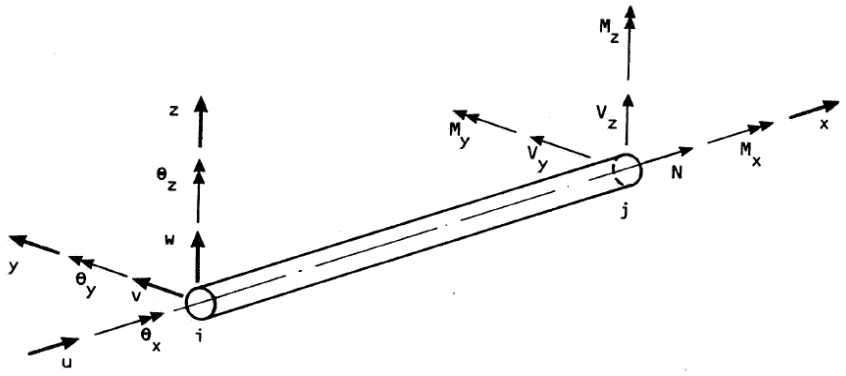

Figure 4.7: Definition of the axis in USFOS for a three dimensional beam element. Reprinted from SINTEF (1988)

One can see the difference from figure 4.6 and figure 4.7. The surge axis corresponds to y-axis defined in USFOS and the sway axis corresponds to the x-axis defined in USFOS. From figure 4.5, the added mass coefficients can be read, see table 4.4.

Motion	**Added mass coefficient**
Sway	0.28
Surge	1.0
Heave	2.3

Table 4.4: The added mass coefficients assigned to the pontoons referring to the definition of motions used for the bridge girder

4.2.3 Cables

The cables connect the tower and the bridge girder. They are modelled as slender beam elements by using hollow pipes as geometry. The detailed design of the cable is not given, in this thesis, the cables are assumed having the same geometry. The geometry of the cable is shown in table 4.5.

Diameter	Thickness	Area
$[mm]$	$[mm]$	$[mm^2]$
138.2	69	0.015

Table 4.5: Cross section properties of cables

Property	Value	Unit
E	206	[GPa]
σ_Y	1860	[MPa]
ρ	100	$[kg/m^3]$

Table 4.6: Material properties of cables

They are flexible elements since they have relatively large length as one element. To ensure that there is no bucking of the cables, the command BEAMTYPE is used to set the cables as risers. In addition, the density of the cables is assumed to be small to avoid the cables having downwards movements due to the gravity, here it is assumed as $100 kg/m^3$.

4.3 Improvement of Original Model

4.3.1 Pre-tension in Cables

In the previous model, there is no tension defined in the cable. When the dead load is applied to the bridge, the bridge will deform until the elongation of the cables are large enough for the forces in the cable to balance the weight. This process makes the balance of the bridge, especially the middle navigation channel part, very difficult to achieve.

To improve the situation, the pre-tension in the cables are introduced to the model. When a structure experiences a temperature lower than a certain level, the structure will produce an axial force. According to Bell (2011), the equation 4.8 can be used to estimate the temperature in the cables.

$$\sigma = E \cdot \lambda \cdot \Delta T \tag{4.4}$$

where E is the elastic modulus, λ is the thermal expansion coefficient and ΔT is the temperature variation. The thermal expansion coefficient used for the cables is shown in table 4.7. Since the balance checking process is very time consuming, the final temperature is obtained until the vertical displacement of the bridge is less than $8cm$. The temperature distribution on different cables is shown in figure 4.8. The temperature ranges from -170 °C to -240 °C.

Thermal expansion coefficient	**Unit**
1.40E-05	[1/°C]

Table 4.7: Thermal expansion coefficient

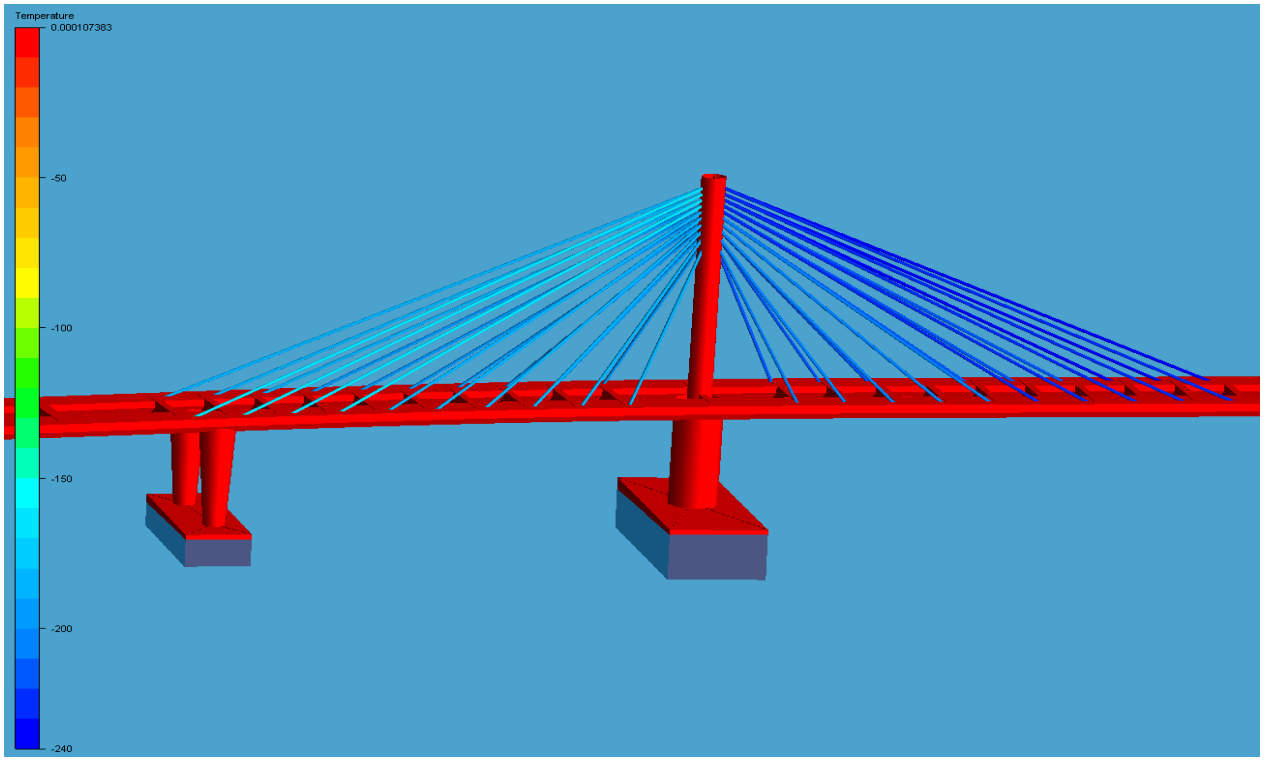

Figure 4.8: Temperature distribution on cables

4.3.2 Balance Check of the Bridge

As mentioned above, there is not enough information about the ballast weight of the pontoons, the weight equilibrium is found by rough estimation of buoyancy and permanent load. The buoyancy of each pontoon is obtained by calculating the volume of the submerged part. The dead weight is calculated by using the volume of the superstructure multiplied by their density. In previous modelling, the pre-tension in the cables is not considered.

When running the dynamic analysis of the bridge itself, ballast weight of several pontoons is not distributed correctly and the middle part of the bridge sinks considerably, one can see from figure 4.9. The figure shows the vertical displacement of the bridge in a scale factor of 10. After adding the pre-tension in the cables, more dynamic simulations are conducted until the correct ballast of the pontoons is achieved and the middle part of the bridge will not sink after adding pre-tension of the cables. Figure 4.10 shows the final equilibrium of the bridge with a variation of $8cm$ regarding to vertical displacement of each pontoon, which is considered as a relatively correct ballast distribution.

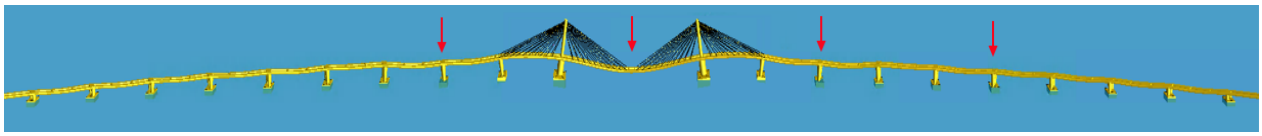

Figure 4.9: Overview of the original ballast distribution. Vertical displacement scaled by 10

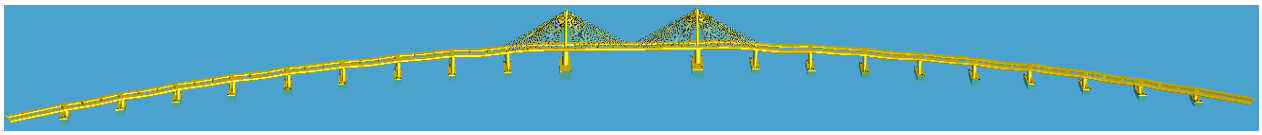

Figure 4.10: Overview of the final ballast distribution. Vertical displacement scaled by 10

4.4 Ship Collision Analysis Setup

The height of the container ship is 18 meters, the height of the bridge deck in the middle is around 51.5 meters. It is unlikely that the ship bulb will hit the bridge deck, so the collision between the ship bulb and pontoon is simulated. Since a ship can sail any direction when it is

going through the navigation channel, several different collision angels between the ship and pontoon are investigated. The different collision scenarios are shown in table 4.8 and figure 4.11.

In USFOS, the ship mass is given to a node mass and the ship is modelled as a non-linear spring that connected to the pontoon by another non-linear spring with hyperelastic material. The hyperelastic material has the property that when it is under compression, the deformation is very small since the spring has infinitely stiffness in compression, on the contrast, the deformation will be large when the spring is in tension due to its zero stiffness. This is necessary to simulate the ship deflection from the pontoon after the collision.

In terms of the spring of the ship, the force deformation curve obtained from LS-DYNA is used to the spring to ensure correct energy distribution between the vessel and the bridge. The two springs are constrained so that they can only have displacement in the transverse direction relative to the bridge, one can see the location of the two springs in figure 4.12.

	Collision Direction	**Collision Energy** [MJ]	**Ship Mass** [ton]	**Ship Speed** [Knots]	**Ship Speed** [m/s]
Scenario 1(SC 1)	0°	158.4	35 200	6	3
Scenario 2(SC 2)	0°	440	35 200	10	5
Scenario 3(SC 3)	180°	440	35 200	10	5
Scenario 4(SC 4)	150°	440	35 200	10	5

Table 4.8: Container ship set up in different scenarios

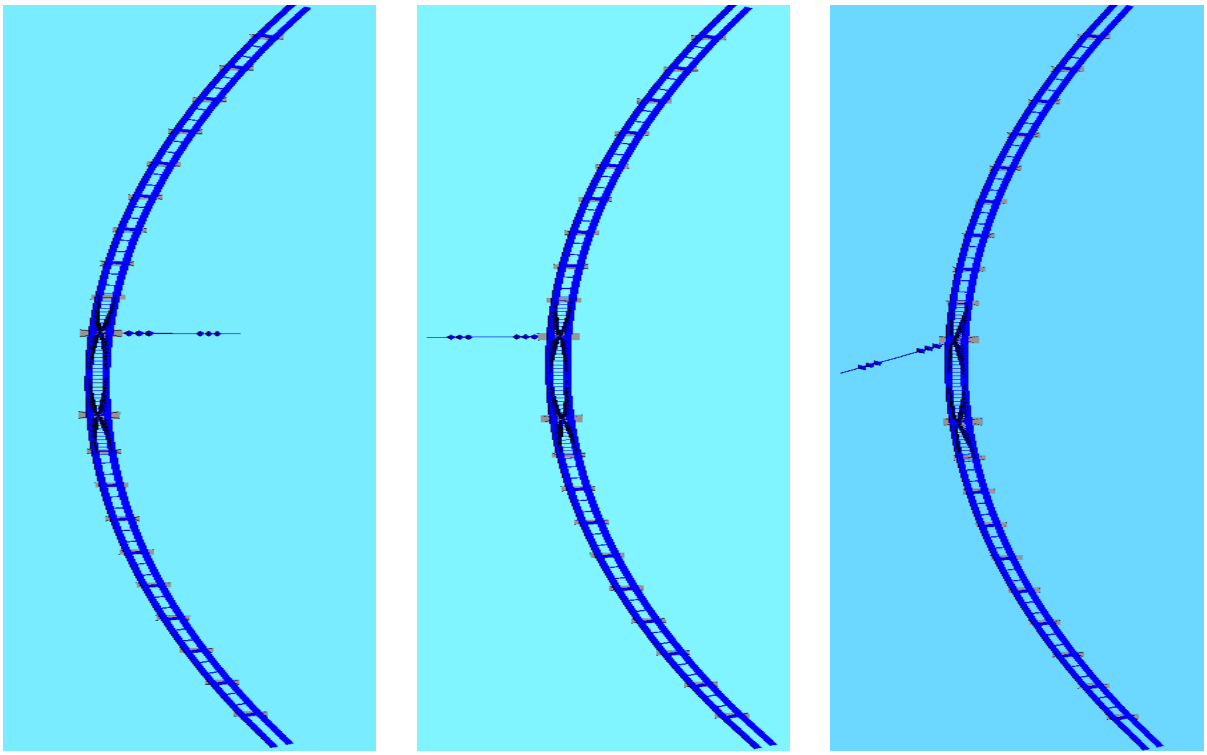

(a) Collision angel 0° (b) Collision angel 180° (c) Collision angel 150°

Figure 4.11: Different angels of ship-pontoon collision

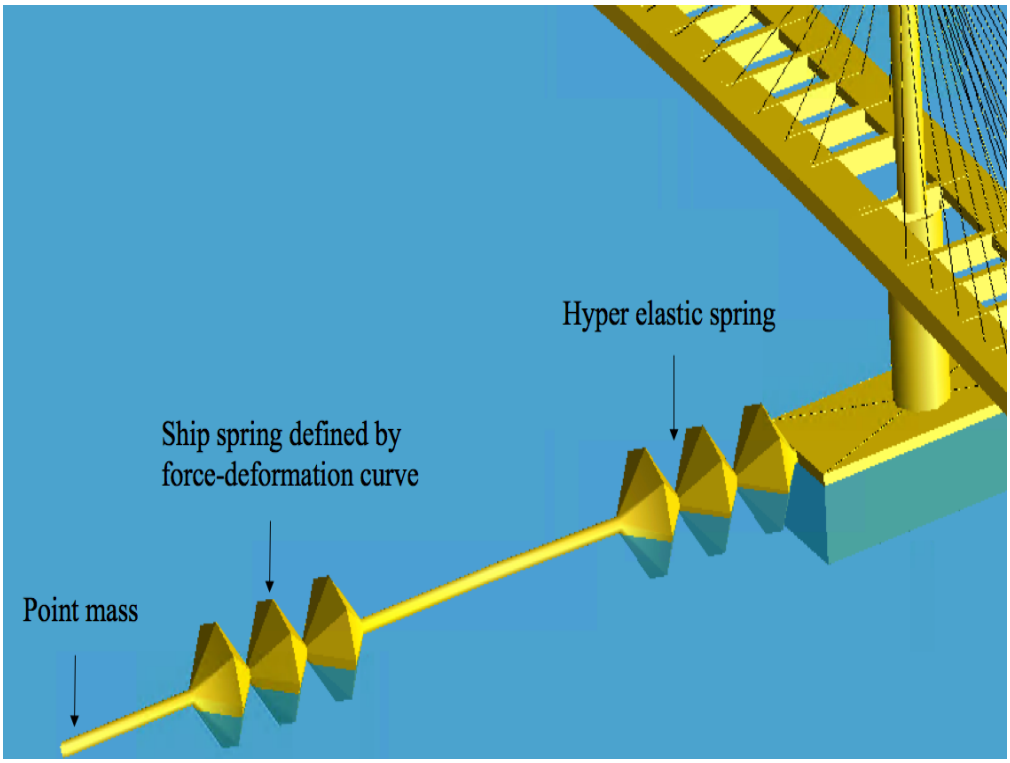

Figure 4.12: Non-linear springs location

The input information of the non-linear spring is the simplification of the force-displacement curve obtained from LS-DYNA mentioned in Chapter 3. The force displacement curve of the proposed relatively safe pontoon is shown in figure 4.13. The simplified curve is used due to the limited input number in USFOS, so several points are picked so that they can represent the original curve. The simplified force deformation curve is shown in figure 4.14.

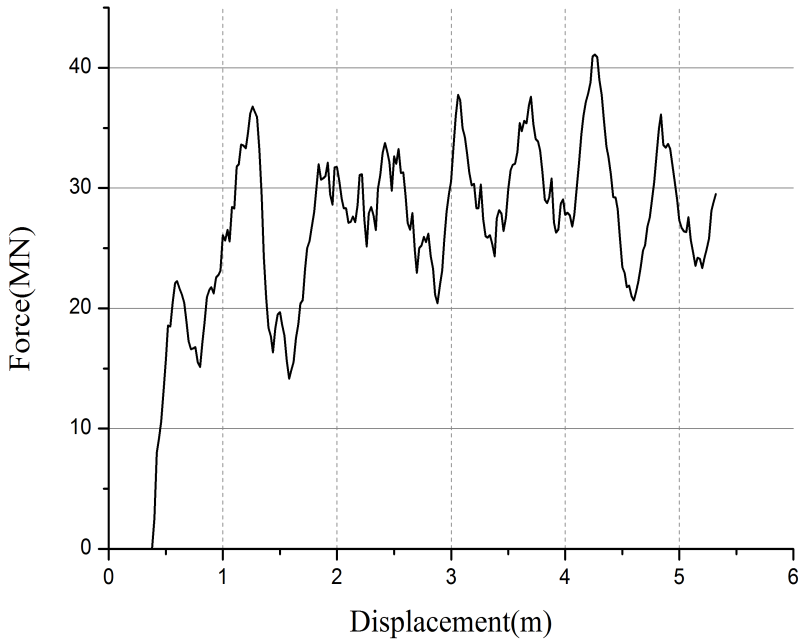

Figure 4.13: The force displacement curve obtained from LS DYNA

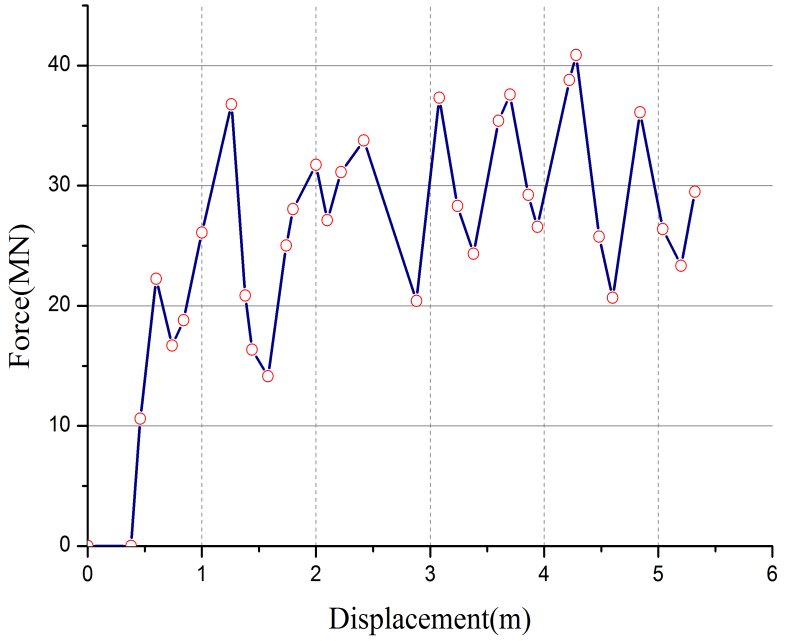

Figure 4.14: The simplified force displacement curve for the input in USFOS

4.5 Results and Discussion

4.5.1 Results of SC 1 and SC 2

Figure 4.15 shows the time history of the transverse displacement of the bridge measured at the contact point in SC 1 and SC 2 in which the ship has the same sailing direction. The maximum transverse displacement of the bridge is approximately 2.4m and 3.4m in SC 1 and SC 2.

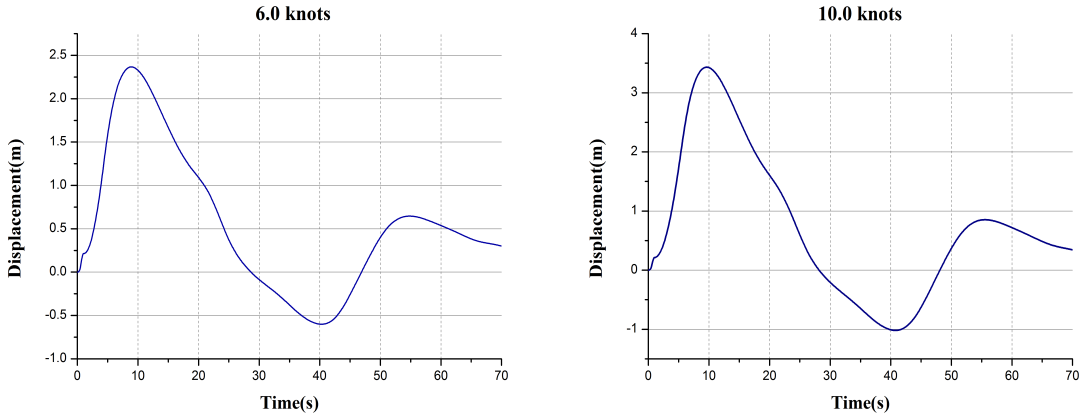

(a) Displacement history in SC 1 (b) Displacement history in SC 2

Figure 4.15: Displacement history of the contact point in SC 1 and SC 2

The contact force between the pontoon and the ship is shown in figure 4.16. It can be seen that the impact time between the ship and the bridge is 4.9s and 6.0s respectively and the maximum contact force is approximately 37MN and 48MN respectively. The contact time t_d is 9.8% and 12% of the natural period T_n, where T_n is about 55s from figure 4.15. The original kinetic energy of the ship is not totally absorbed by the bridge, so the the ship will drift away after collision.

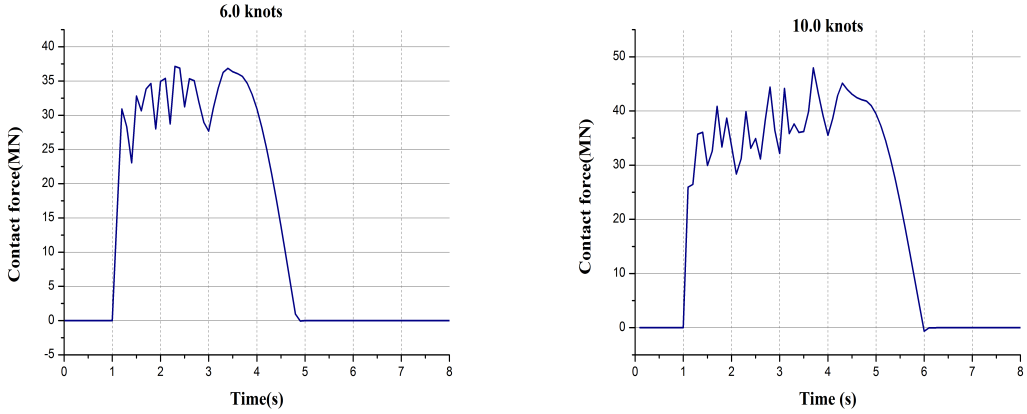

(a) Contact force in SC 1 (b) Contact force in SC 2

Figure 4.16: Contact force between the pontoon and the ship in SC 1 and SC 2

Figure 4.17 shows the deformation history of the non-linear spring which is used to represent the ship. The spring has a permanent deformation after the collision, the values are around 3.2m and 8.8m in SC 1 and SC 2 respectively.

The force deformation curve of the non-linear spring representing the ship is shown in figure 4.18. The area under the curve is the strain energy that absorbed by the ship during the collision, one can estimate the area from the figure. The approximate area under the curve are 105MJ and 315MJ respectively. The absorbed energy accounts for 66% and 72% of the initial collision energy, meaning the energy that the bridge absorbed is around 53.4MJ and 125MJ in the two cases.

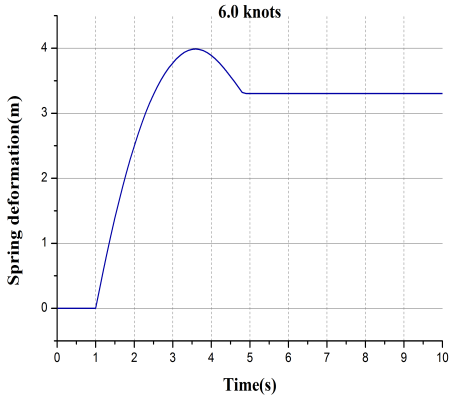

(a) Ship spring deformation in SC 1

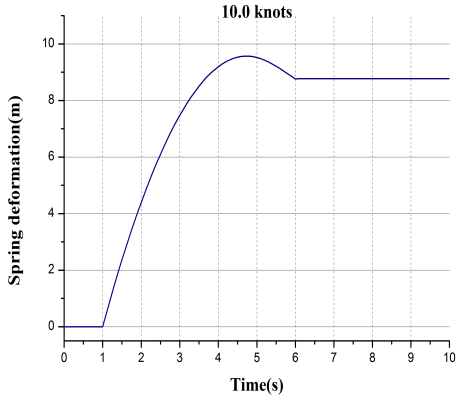

(b) Ship spring deformation in SC 2

Figure 4.17: Ship spring deformation history in SC 1 and SC 2

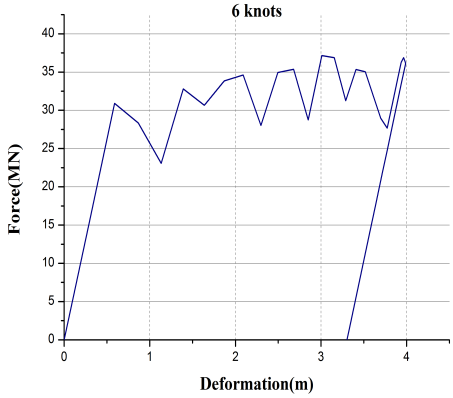

(a) Force deformation curve in SC 1

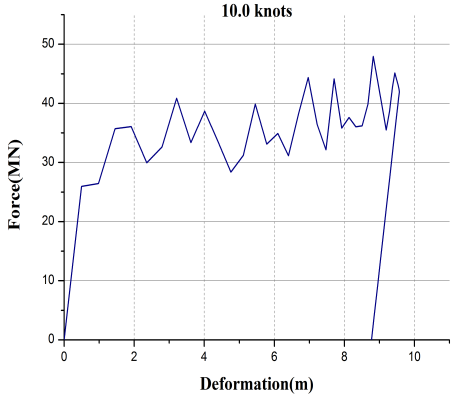

(b) Force deformation curve in SC 2

Figure 4.18: Force deformation curve in SC 1 and SC 2

The most critical state for the bridge girder can be found when it has the maximum transverse displacement. The bridge deck that right upon the ship at this time point is investigated, see figure 4.19. The forces of this deck at this time point in SC 1 and SC 2 are listed in table 4.9. The maximum forces of the bridge girder in these two cases is shown in table 4.10. From figure 4.9 one can see that the difference in the forces is not very large, in SC 2, the forces and the moments are a little larger than that in SC 1. The transverse bending moment M_z in these two cases is large compared to other values, which is reasonable since the ship-bridge collision occurs at the middle point of the bridge, it is easy to trigger large transverse bending moment. In addition,

the transverse bending mode will be governed by a half wave eigenmode.

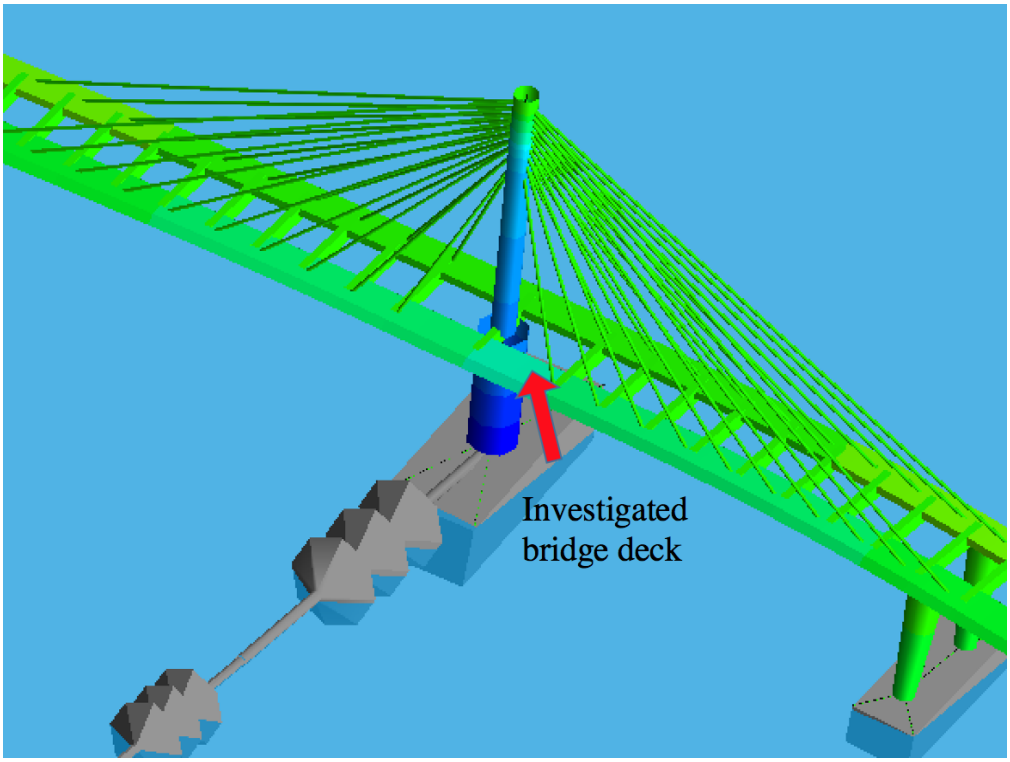

Figure 4.19: The investigated bridge deck when the bridge has the maximum transverse displacement. Scaled by factor 10

	F_x [MN]	F_y [MN]	F_z [MN]	M_x [MNm]	M_y [MNm]	M_z [MNm]
SC 1	9	5.5	11	50	15	-320
SC 2	10	6.5	13	100	16	-450

Table 4.9: The forces of the investigated bridge deck in SC 1 and SC 2

	SC 1	SC 2
Axial force F_x(Compression)	90MN	100MN
Transverse shear force F_y	8MN	11MN
Lateral shear force F_z	12MN	14MN
Torsional moment M_x	100MNm	120MNm
Lateral bending moment M_y	18MNm	24MNm
Transverse bending moment M_z	400MNm	550MNm

Table 4.10: The maximum forces of the bridge deck in SC 1 and SC 2

4.5.2 Results of SC 3 and SC 4

The results obtained from Scenario 3 and Scenario 4 are shown in the following figures.

In figure 4.20, it shows the transverse displacement of the bridge. The maximum displacement of the bridge is around 3.3m in SC 3 and 2.5m in SC 4. Compared to SC 1 and SC 2, the direction of the maximum displacement has changed since the ship sailing direction changed.

The contact force between the pontoon and the ship in SC 3 and SC 4 is shown in figure 4.21. The contact time between the ship and the bridge is 5.5s and 6.3s respectively. It can be calculated that the contact time is 11% and 12.6% of the natural period T_n, where T_n is about 50s from figure 4.20.

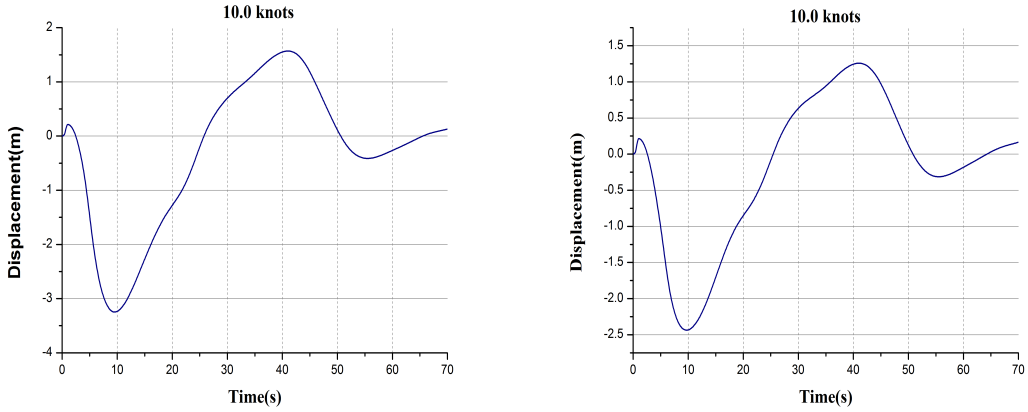

(a) Displacement history in SC 3 (b) Displacement history in SC 4

Figure 4.20: Displacement history of the contact point in SC 3 and SC 4

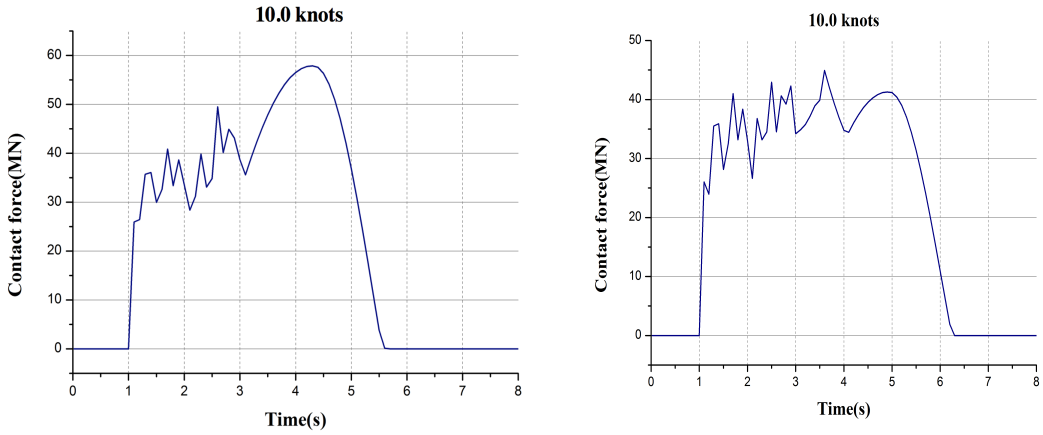

(a) Contact force in SC 3 (b) Contact force in SC 4

Figure 4.21: Contact force between the pontoon and the ship in SC 3 and SC 4

Figure 4.22 shows the deformation history of the non-linear spring representing the ship in SC 3 and SC 4. The spring has a permanent deformation after the collision, the deformation value is 8m and 9m respectively.

The force deformation curve of the non-linear spring representing the ship is shown in figure 4.23. The area under the curve is approximately 280MJ and 315MJ, meaning the ship absorbs 280MJ and 315MJ energy during the collision. The absorbed energy accounts for around 67% and 71.6% of the total initial energy, so the energy that the bridge absorbed is 160MJ and 125MJ respectively.

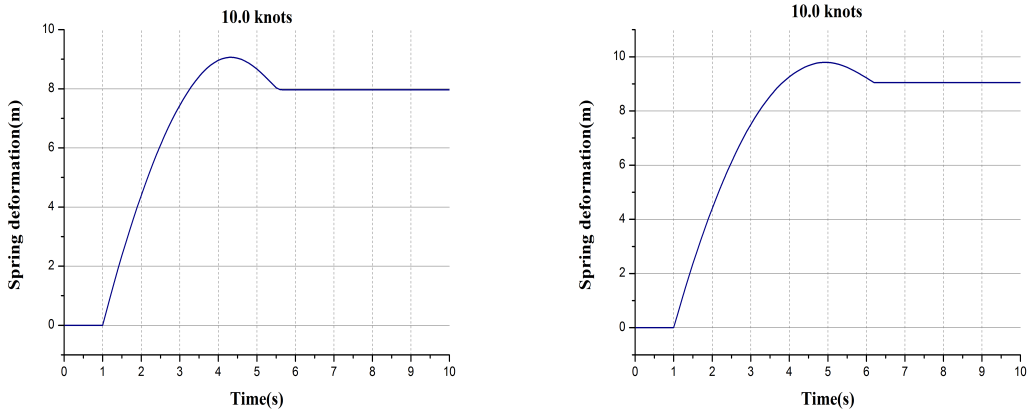

(a) Ship spring deformation in SC 3 (b) Ship spring deformation in SC 4

Figure 4.22: Ship spring deformation history in SC 3 and SC 4

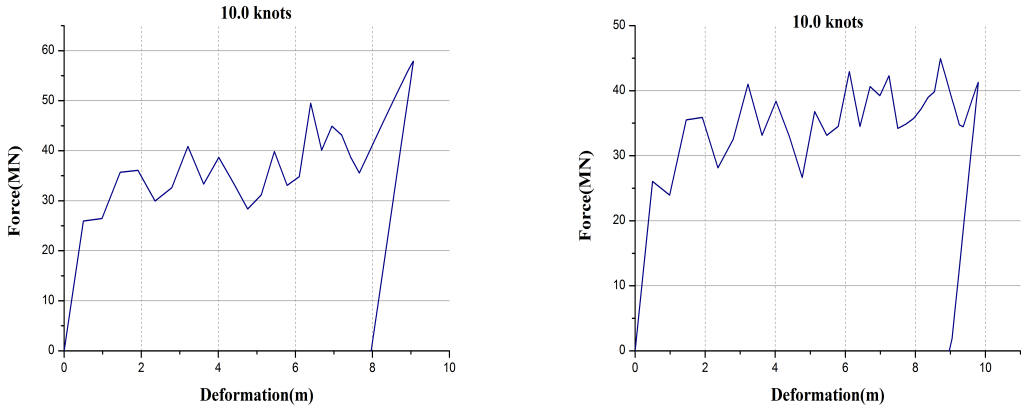

(a) Force deformation curve in SC 3 (b) Force deformation curve in SC 4

Figure 4.23: Force deformation curve in SC 3 and SC 4

Similar to the SC 1 and SC 2, the bridge has the maximum transverse displacement when the speed of the ship reduces to zero. The forces of the investigated bridge deck at this time point is shown in table 4.11. The maximum forces of the bridge is shown in table 4.12. Similar to SC 1 and SC 2, these two cases mainly subject to the transverse bending as well. The forces and moments are quite similar in SC 3 and SC 4. It should be noticed that the torsional moment M_x is larger compared with the values in SC 1 and SC 2.

	F_x [MN]	F_y [MN]	F_z [MN]	M_x [MNm]	M_y [MNm]	M_z [MNm]
SC 3	10	6.5	3	-300	-24	450
SC 4	11	3.7	3.5	-250	-30	320

Table 4.11: The forces of the investigated bridge deck in SC 3 and SC 4

	SC 3	SC 4
Axial force F_x(Compression)	71MN	70MN
Transverse shear force F_y	11MN	12MN
Lateral shear force F_z	10MN	10MN
Torsional moment M_x	300MNm	260MNm
Lateral bending moment M_y	25MNm	30MNm
Transverse bending moment M_z	550MNm	400MNm

Table 4.12: The maximum forces of the bridge deck in SC 3 and SC 4

The axial stress of two cables are investigated in SC 3 and SC 4. One cable(Cable 2) is the shortest cable which locates the nearest to the ship collision point, one cable(Cable 1) is the longest cable which locates away from the collision point. The axial stress of the two cables are shown in figure 4.24. At the beginning(0-1s), the axial stress goes sharply from zero to a relatively large value because during this period, the pre-tension is being added to the cables. It can be observed that in both cases that cable 1 goes to stable when the stress goes to 600MPa and the cable 2 becomes stable at around 450MPa. The largest axial stress in the cable happens at 9s in cable 2, around 750MPa, is 20% and 40% larger than the stable stress. The cables of the suspension bridge are normally made by high strength steel with the yield stress 1180MPa according to Gimsing and Georgakis (2011) and the yield stress that defined in this thesis is 1860MPa for the cables. The defined yield stress is 59% higher than the largest value of the stress and the stable stress has little trend to change in a large scale, so the stresses in the cables can be considered as safe design in this case. All the other cables behave more or less the same with these two investigated cables.

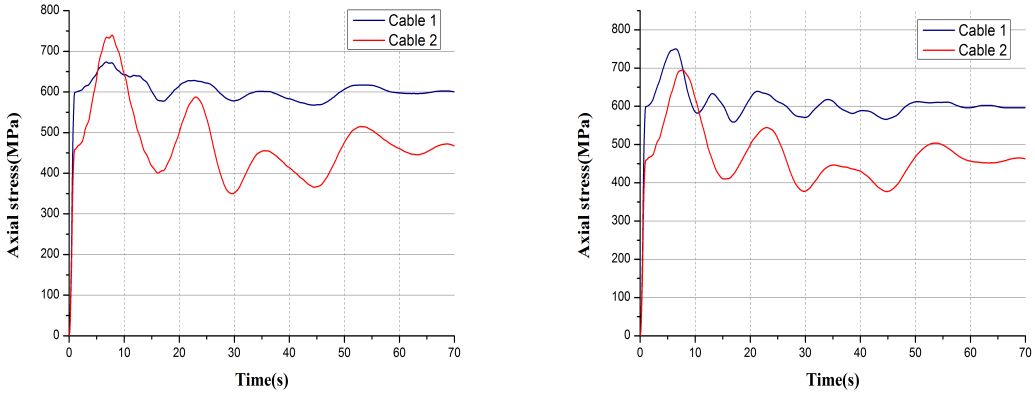

(a) Axial stress in cables in SC 3

(b) Axial stress in cables in SC 4

Figure 4.24: Axial stress in cables in SC 3 and SC 4

4.5.3 Discussion

Some assumptions in terms of the geometry and the properties of the structures are made during modelling. The cables are assumed to have a large elastic modulus and high yield stress in order to avoid buckling behavior, the density of the cables are assumed to be small in order to minimize the gravity effect. The effect of the large elastic modulus and the yield stress on the eigenperiod is uncertain.

It is proved that the improvements made for the previous bridge are useful, including adding pre-tension in the cables and rechecking the balance of the bridge with considering the pre-tension in cables. In the project thesis Wang (2016), the hand calculation of the maximum displacement of the bridge is 3.2m when the ship speed is 10.0 knots. The maximum transverse displacement of the bridge calculated in USFOS in scenario 2(ship speed 10.0 knots) is 3.4m. The two values correspond quite well meaning the improvements of the original bridge have a positive effect.

In these cases, the bridge subjects mainly the transverse bending moment M_z. The relatively larger stresses occur at the collision point and the ends of the bridge. If the ship speed increases, there is a possibility that the transverse bending moment will exceed the design bending moment. Larger ship speeds are suggested to simulate the collision.

In terms of SC 4, the ship-pontoon collision happens in a different angel with the same speed in SC 3. However, the results of SC 4 have little difference compared with the results of SC 3, one can see the results in table 4.12. The torsional moment M_x and transverse bending moment M_z are smaller than the results of SC 3, which is reasonable since the component of the speed in y direction in SC 4 would be smaller than the speed in SC 3.

Chapter 5

Conclusion

5.1 Conclusion

5.1.1 Local Ship Bow-Pontoon Collision Analysis

A pontoon steel design that is highly resistant against ship collision is proposed. The finite element model of the pontoon was built in LS-DYNA, the strength of the base model was improved by increasing the thickness of the girders, ring stiffeners and adding three more ring stiffeners. The base design of the pontoon can resist the forecastle well, however, the ship bow can penetrate into the pontoon easily. In terms of resisting the ship bow, it is proved that either only increase the thickness of the girders and ring stiffeners or only add ring stiffeners has little effect of resisting the ship bow collision. Even though more energy is absorbed by the ship under these conditions, the energy of the pontoon is still large expect the proposed pontoon design with absorbing 12MJ energy, which can be considered as a relatively safe design. The safe pontoon has the additional ring stiffeners and the thicker girders and ring stiffeners as well. The peak forces corresponding to the original pontoon and the proposed pontoon are 26MN and 42MN respectively.

The force-deformation curve was obtained by simulating the ship-pontoon collision in LS-DYNA. The force-deformation curve can be divided into two curves, one is for the bulb and one is for

the forecastle. Considering the height of the bridge deck in the middle navigation channel, it is practical to use the bulb curve to define the non-linear spring representing the ship.

5.1.2 Global Analysis of the Bridge

The response of the bridge is investigated in different ship collision situations. The design of the bridge is still in early stage, the detailed information of the bridge is not given, so it is quite hard to conclude the bridge is safe or not under the condition of ship collision, however one can refer to Chapter 4 to see the results in different collision situations. In the investigated cases, the bridge is proved quite safe after experiencing the collision.

The maximum transverse displacement in these cases is 3.5m, which can be considered as a small deflection compared with the length of the bridge. The displacement in USFOS simulation is close to the value obtained from the hand calculation of the single degree of freedom.

The axial stress in the cables is investigated. The stress increases significantly at the beginning due to the pre-tension is acting in the cables, then the stress goes to a steady level. The cables are safe because the maximum stress in the cables is around 60% less than the yield stress.

Chapter 6

Suggestions for Future Work

Improvement of the finite element model can be made. A more mesh converged model of the ship bow and the pontoon can be improved to obtain a more trustworthy force deformation curve. To maximize economic benefits, further investigation can be conducted by using normal steel applied to the pontoon parts that have little contribution to the force deformation curve. In addition, it is not necessary to increase the thickness of the rings that is near the forecastle part, the effect of this condition can be checked as future work. The finite element model of the bridge in USFOS can also be improved by using different diameter for different cables, the pre-tension in the cables could be further improved.

There is a possibility that even with the strong design of the pontoon, damage happens during the collision. It is recommended that the flooding situation of the pontoon should be simulated to see the response of the bridge.

The environmental load is very important for the bridge design. In this thesis, due to lack of time the environmental load such as wind load and wave load is not investigated in detail. The dynamic analysis of the ship-bridge collision under extreme environmental loads can be regarded as future work.

Bibliography

Bell, K. (2011). Matrix statistics: statistical calculations of frame structures.

COWI (2016). Curved bridge-navigation channel in south,2016.

DNV-OS-B101 (April 2016). *Design of offshore steel structures, general - LRFD method*.

DNV-RP-C204 (2010). Design against accidental loads, october 2010.

Eldegard, O. (2016). *Analysis and Design of Floating Bridge over Bjørnefjorden Subjected to Large Ship Collisions*. PhD thesis, Norwegian University of Science and Technology, Norway.

Gimsing, N. J. and Georgakis, C. T. (2011). *Cable supported bridges: concept and design*. John Wiley & Sons.

Hagiwara, K., Takanabe, H., and Kawano, H. (1983). A proposed method of predicting ship collision damage. *International Journal of Impact Engineering*, 1(3):257–279.

Haris, S. and Amdahl, J. (2013). Analysis of ship–ship collision damage accounting for bow and side deformation interaction. *Marine Structures*, 32:18–48.

Hong, L. and Amdahl, J. (2008). Crushing resistance of web girders in ship collision and grounding. *Marine Structures*, 21(4):374–401.

Moan, T. (2003). Finite element modelling and analysis of marine structures. *Department of Marine Technology, NTNU*.

Ohtsubo, H., Kawamoto, Y., and Kuroiwa, T. (1994). Experimental and numerical research on ship collision and grounding of oil tankers. *Nuclear engineering and design*, 150(2):385–396.

Petersen, M. J. (1982). Dynamics of ship collisions. *Ocean Engineering*, 9(4):295–329.

SINTEF (1988). Usfos theory manual.

Storheim, M. (2016). *Structural response in ship-platform and ship-ice collisions*. PhD thesis, PhD thesis, Norwegian University of Science and Technology, Norway.

Tabri, K., Broekhuijsen, J., Matusiak, J., and Varsta, P. (2009). Analytical modelling of ship collision based on full-scale experiments. *Marine Structures*, 22(1):42–61.

Tore H. Soreide, Jorgen Amdahl, E. E. T. H. and Hellam, O. (1993). Usfos - a computer program for progressive collapse analysis of steel offshore structure. theory manual.

Vegvesen, S. (2015). Ferjefri e39 bruutforming og nye løysingar, visited 10.11.2016.

Vredeveldt, A. and Wevers, L. (1993). Full scale ship collision tests.

Wang, B. (2016). *Analysis and Design Bjørnefjorden Floating Cable-Stayed Bridge subjected to Large Ship Collisions and Extreme Environmental Loads*. PhD thesis, Norwegian University of Science and Technology, Norway.

Wang, Z. (2000). The current status and trend of ship collision. *Shipbuilding technology*, (4):7–12.

Appendix A

Matlab transcript

A.1 Coordinate calculation

```
%%%%%%%%%%%%%%%%%%%%%%%%%%%%%%%%%%%%%%%%%%%%%%%%%%%%%%%%%%%%%%%%%%%%%%%
% This script is the calculation of x-, y-, z- coordinate values
%%%%%%%%%%%%%%%%%%%%%%%%%%%%%%%%%%%%%%%%%%%%%%%%%%%%%%%%%%%%%%%%%%%%%%%
clc
close all
clear all
format short
%% the x,y value
Rv=53243;    %m;
h0=52;      %m;
rv=Rv-h0;     %m
Rh=4802;
theta=4198/2/Rh;
L=Rh*cos(theta);
L1=Rh-L;

theta11=225/Rh;
x11=Rh*sin(theta11);
y11=Rh*cos(theta11)-L;
z11=sqrt(Rv^2-x11^2)-rv;

theta12=(225+200)/Rh;
x12=Rh*sin(theta12);
y12=Rh*cos(theta12)-L;

Lmid=225+200:186:4198/2;  %the curve length of each part
for i=1:10
    theta(i)=Lmid(i)/Rh;
    x(i)=Rh*sin(theta(i));
    y(i)=Rh*cos(theta(i))-L;
    z(i)=sqrt(Rv^2-x(i)^2)-rv;  % height of the colomn.
    X=[x11,x];   % X value for 11 to 21
    Y=[y11,y];   % Y value for 11 to 21
    Z=[z11,z];   % Z value for 11 to 21
end
XYZ=[X;Y;Z];

%% the points on the pontoon
% No.11
H11=98;    B11=39;    T11=23;  % the NO11 pontoon geo
H12_20=79;  B12_20=26;         % geo of NO12 to NO20
P1101=[x11,y11,3];            % center of the NO11 pontoon
P11001=[x11+B11/2,y11+H11/2,3];
P11002=[x11-B11/2,y11+H11/2,3];
P11003=[x11+B11/2,y11-H11/2,3];
P11004=[x11-B11/2,y11-H11/2,3];
%NO.12 to NO.20 center point of the pontoon
P1201=[X(2),Y(2),3];
P1301=[X(3),Y(3),3];
P1401=[X(4),Y(4),3];
P1501=[X(5),Y(5),3];
P1601=[X(6),Y(6),3];
P1701=[X(7),Y(7),3];
P1801=[X(8),Y(8),3];
P1901=[X(9),Y(9),3];
P2001=[X(10),Y(10),3];
% 6 points of the NO:12 pontoon
```

```
h_col=(50-9)/2;        % distance betwenn the colunms center
P12001=[X(2)+B12_20/2,Y(2)+H12_20/2,3];
P12002=[X(2)-B12_20/2,Y(2)+H12_20/2,3];
P12003=[X(2)+B12_20/2,Y(2)-H12_20/2,3];
P12004=[X(2)-B12_20/2,Y(2)-H12_20/2,3];
P12005=[X(2)+h_col*sin(theta12),Y(2)+h_col*cos(theta12),3]; % the
column center1
P12006=[X(2)-h_col*sin(theta12),Y(2)-h_col*cos(theta12),3]; % the
column center2
% x value for 001 ,002,003,004 points on the pontoons NO.13 to NO.20
for j=1:8
    x001(j)=P12001(1)+x(j+1)-x(1); %x001(1)is the point on NO.13
    x003(j)=x001(j);
    x002(j)=P12002(1)+x(j+1)-x(1);
    x004(j)=x002(j);
end
% y value for 001 ,002,003,004 points on the pontoons NO.13 to NO.20
for j=1:8
    y001(j)=y(j+1)+H12_20/2;    %y001(1)is the point on NO.13
    y002(j)=y001(j);
    y003(j)=y(j+1)-H12_20/2;
    y004(j)=y003(j);
end
%4 edge points on the pontoons No.13 to NO.20
for j=1:8
    P001(j,:)=[x001(j)',y001(j)',3];
    P002(j,:)=[x002(j)',y002(j)',3];
    P003(j,:)=[x003(j)',y003(j)',3];
    P004(j,:)=[x004(j)',y004(j)',3];
end
% Center points of the colunms on pontoons NO13 to NO20
for j=1:8
P005(j,:)=[x(j+1)+h_col*sin(theta(j+1)),y(j+1)+h_col*cos(theta(j+1)),3]
; % the column center
P006(j,:)=[x(j+1)-h_col*sin(theta(j+1)),y(j+1)-
h_col*cos(theta(j+1)),3]; % the column center
end
% The beams between the bridges
L_b=425+62:62:4198/2-186;
l_b=41;      %geo of the beam between the bridge
for k=1:24
theta_b(k)=L_b(k)/Rh;
x_b(k)=Rh*sin(theta_b(k));
y_b(k)=Rh*cos(theta_b(k))-L;
z_b(k)=sqrt(Rv^2-x_b(k)^2)-rv;
P_b(k,:)=[x_b(k)',y_b(k)',z_b(k)'];  % the center of the beam
x_b0025_0048(k)=x_b(k)+l_b/2*sin(theta_b(k));
y_b0025_0048(k)=y_b(k)+l_b/2*cos(theta_b(k));
P_b0025_0048(k,:)=[x_b0025_0048(k)',y_b0025_0048(k)',z_b(k)']; % 0025
to 0048
x_b20025_20048(k)=x_b(k)-l_b/2*sin(theta_b(k));
y_b20025_20048(k)=y_b(k)-l_b/2*cos(theta_b(k));
P_b20025_20048(k,:)=[x_b20025_20048(k)',y_b20025_20048(k)',z_b(k)']; %2
0025 to 20048
end
%% Cable positions
L_c=10:20:10+180;
l_c=41;  % equal to the beam between the bridge.
```

```
L_c1=260:20:260+180;
for n=1:10
    theta_c(n)=L_c(n)/Rh;
    x_c(n)=Rh*sin(theta_c(n));
    y_c(n)=Rh*cos(theta_c(n))-L;
    z_c(n)=sqrt(Rv^2-x_c(n)^2)-rv;
    P_c(n,:)=[x_c(n)',y_c(n)',z_c(n)']; %center of the cable
    x_c03021_03030(n)=x_c(n)+l_b/2*sin(theta_c(n));
    y_c03021_03030(n)=y_c(n)+l_b/2*cos(theta_c(n));

P_c03021_03030(n,:)=[x_c03021_03030(n)',y_c03021_03030(n)',z_c(n)']; %
03021 to 03030
    x_c01021_01030(n)=x_c(n)-l_b/2*sin(theta_c(n));
    y_c01021_01030(n)=y_c(n)-l_b/2*cos(theta_c(n));

P_c01021_01030(n,:)=[x_c01021_01030(n)',y_c01021_01030(n)',z_c(n)'];%
01021 to 01030

   % 03031 to 03040; 01031 to 01040
    theta_c1(n)=L_c1(n)/Rh;
    x_c1(n)=Rh*sin(theta_c1(n));
    y_c1(n)=Rh*cos(theta_c1(n))-L;
    z_c1(n)=sqrt(Rv^2-x_c1(n)^2)-rv;
    P_c1(n,:)=[x_c1(n)',y_c1(n)',z_c1(n)']; %center of the cable
    x_c03031_03040(n)=x_c1(n)+l_b/2*sin(theta_c1(n));
    y_c03031_03040(n)=y_c1(n)+l_b/2*cos(theta_c1(n));

P_c03031_03040(n,:)=[x_c03031_03040(n)',y_c03031_03040(n)',z_c1(n)']; %
03031 to 03040
    x_c01031_01040(n)=x_c1(n)-l_b/2*sin(theta_c1(n));
    y_c01031_01040(n)=y_c1(n)-l_b/2*cos(theta_c1(n));

P_c01031_01040(n,:)=[x_c01031_01040(n)',y_c01031_01040(n)',z_c1(n)'];%
01031 to 01040
end
%the tower
P_top=[x11,y11,155]; % toppest point on the tower
z_t=155-3.5:-2.5:155-3.5-22.5;
for  n=1:10
P_t(n,:)=[x11,y11,z_t(n)'] % points on the tower
end
```